Journal of Inorganic Biochemistry 201 (2019) 110822

Contents lists available at ScienceDirect

Journal of Inorganic Biochemistry

journal homepage: www.elsevier.com/locate/jinorgbio

# Design, synthesis and biological evaluation of iridium(III) complexes as potential antitumor agents

Fan Du[a], Lan Bai[a], Miao He[a], Wen-Yao Zhang[a], Yi-Ying Gu[a], Hui Yin[b,*], Yun-Jun Liu[a,*]

[a] School of Pharmacy, Guangdong Pharmaceutical University, Guangzhou 510006, PR China
[b] Department of Microbiology and Immunology, Guangdong Pharmaceutical University, Guangzhou 510006, China

ARTICLE INFO

*Keywords:*
Iridium(III) complexes
BSA-binding
Cytotoxic activity in vitro and in vivo
Cell invasion
Lysosomes and mitochondria

ABSTRACT

Cisplatin and its analogs have been used for the treatment of various cancers, but their serious side effect has limited clinical application. Presently, scientists are developing other metal drugs as an alternative of cisplatin. In this paper, three new iridium(III) complexes $[Ir(ppy)_2(adppz)](PF_6)$ (adppz = 7-aminodipyrido[3,2-*a*:2′,3′-*c*] phenazine; ppy = 2-phenylpyridine **1**), $[Ir(bzq)_2(adppz)](PF_6)$ (bzq = benzo[*h*]quinolone **2**) and $[Ir(piq)_2(adppz)](PF_6)$ (piq = 1-phenylisoquinoline **3**) were synthesized and characterized. The complexes can effectively inhibit the cell colonies. The cytotoxicity in vitro of the complexes against A549, HepG2, SGC-7901, BEL-7402 and normal NIH3T3 cells was evaluated by 3-(4,5-dimethylthiazole)-2,5-diphenyltetraazolium bromide (MTT) methods. The intracellular reactive oxygen species (ROS) levels and $Ca^{2+}$ concentrations were assayed. The mitochondrial membrane potential, a release of cytochrome *c* and the expression of B-cell lymphoma/leukemia-2 (Bcl-2) family protein have been investigated. The data reveal that the complexes **1**–**3** can effectively inhibit the cell proliferation in A549 cells with low $IC_{50}$ value of 3.2 ± 0.4 μM, 4.8 ± 0.5 μM and 1.2 ± 0.2 μM, respectively. The antitumor in vivo shows that complex **3** can inhibit tumor growth with an inhibitory rate of 76.34%. The studies on the mechanism indicate that these complexes cause apoptosis in A549 cell via a ROS-mediated lysosomal-mitochondrial dysfunction pathway. In addition, the interaction of the complexes with BSA was explored.

## 1. Introduction

Cancer has become one of the major diseases that endanger human health. Its incidence is getting higher and higher, and the mortality rate remains high [1–3]. It is one of the most difficult diseases to cure today. Lung cancer is one of the highest incidence among all malignancy in China, and it is also the “first killer” of cancer death. At present, chemotherapy is the main method for treating most cancers, and the most widely used treatment for lung cancer is cisplatin. Since Rosenberg first discovered that cisplatin has antitumor activity, platinum metal drugs have become one of the most active research and development fields, among which cisplatin, carboplatin and oxaliplatin have been widely used as anticancer drugs, but due to their high toxicity and adverse side effects, which triggered people to seek different metal anticancer drug as alternatives of cisplatin [4–19]. In recent year, the studies of iridium (III) complexes as potent anticancer reagents have triggered extensively interest. So far, a lot of iridium(III) complexes exhibit unique anticancer activity [20–30]. In our previous work, we reduced $-NO_2$ into $-NH_2$, the corresponding ruthenium(II) complexes reveal higher cytotoxic activity than the complexes containing $-NO_2$ [31,32]. In particular, the $IC_{50}$ values of complex $[Ru(dmp)_2(NHPIP)](ClO_4)_2$ containing $-NO_2$ toward BEL-7402, HeLa, MCF-7 and MG-63 cells are 12.4 ± 1.4, 18.5 ± 2.1, 15.5 ± 1.2 and 16.9 ± 1.7 μM. However, the $-NO_2$ was reduced into $-NH_2$, the complexes $[Ru(dmp)_2(AHPIP)](ClO_4)_2$ (dmp = 2,9-dimethyl-1,10-phenanthroline, AHPIP = 2-(3-amino-4- hydroxylphenyl)imidazo [4,5-*f*][1,10]phenanthroline) show higher anticancer activity and the $IC_{50}$ values are 5.4 ± 0.5, 6.8 ± 0.7, 5.1 ± 0.4 and 6.5 ± 0.4 μM against the above cancer cell lines [32]. Thus, we consider reducing $-NO_2$ into $-NH_2$, the anticancer activity of the complexes will be enhanced. Additionally, the ruthenium(II) complexes $[Ru(dmp)_2(adppz)](ClO_4)_2$ (adppz = 7-aminodipyrido[3,2-*a*:2′,3′-*c*]phenazine) also display high anticancer effect on A549, BEL-7402, MG-63 and SKBR-3 cells [33]. In our recent work, we found that $[Ir(piq)_2(ndppz)](PF_6)$ (ndppz = 7-nitrodipyrido[3,2-*a*:2′,3′-*c*]phenazine) with $-NO_2$ as substituent group shows high anticancer activity against A549 cells with an $IC_{50}$ value of 3.4 ± 0.2 μM [34]. The obtained above information stimulates us to reduce $-NO_2$ to $-NH_2$, further explore the anticancer activity. Hence, in this paper, we reduced $-NO_2$ into $-NH_2$, and

* Corresponding authors.
*E-mail addresses:* huiyin0103@gdpu.edu.cn (H. Yin), lyjche@gdpu.edu.cn (Y.-J. Liu).

https://doi.org/10.1016/j.jinorgbio.2019.110822
Received 12 June 2019; Received in revised form 2 September 2019; Accepted 2 September 2019
Available online 04 September 2019
0162-0134/ 

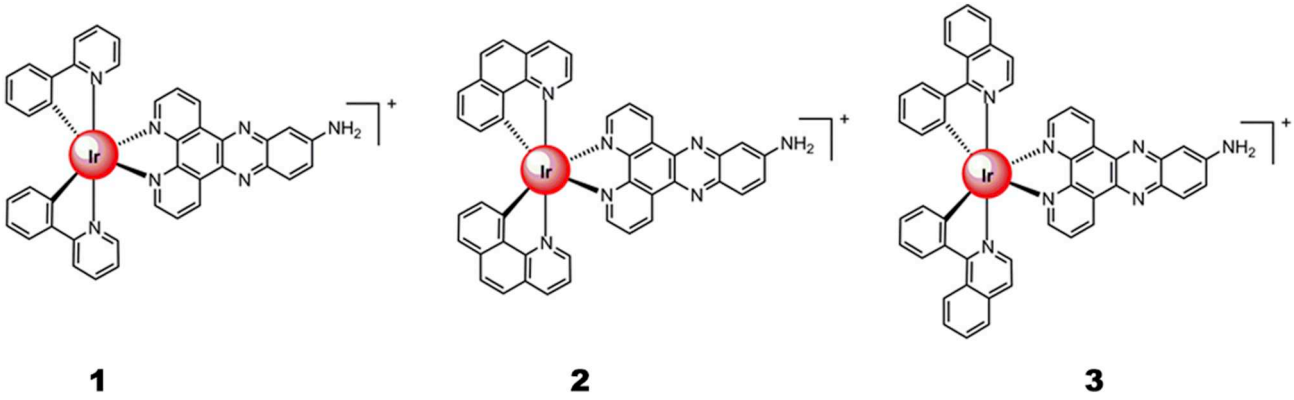


1 2 3

**Scheme 1.** Structures of complexes **1**, **2** and **3**

corresponding three new iridium(III) complexes: $[Ir(ppy)_2(adppz)](PF_6)$ (**1**) (ppy = 2-phenylpyridine, adppz = 7-aminodipyrido[3,2-*a*:2′,3′-*c*]phenazine), $[Ir(bzq)_2(adppz)](PF_6)$ (**2**) (bzq = benzo[*h*]quinolone) and $[Ir(piq)_2(adppz)](PF_6)$ (**3**) (piq = 1-phenylisoquinoline, Scheme 1) were prepared and characterized by elemental analysis, ESI-MS, $^1H$ NMR and $^{13}C$ NMR. The cell viability of A549, HepG2, SGC-7901, BEL-7402 and normal NIH3T3 cells induced by the complexes was evaluated by 3-(4,5-dimethylthiazole)-2,5-diphenyltetraazolium bromide (MTT) methods. The complexes show high inhibitory effect on cell growth in A549 cells, the $IC_{50}$ values are 3.2 ± 0.4 for **1**, 4.8 ± 0.5 for **2** and 1.2 ± 0.2 μM for **3**, respectively. The intracellular reactive oxygen species, mitochondrial membrane potential, intracellular $Ca^{2+}$ levels, release of cytochrome *c*, apoptosis induced by the complexes was investigated under fluorescence microscope. The cell cycle distribution was assayed by flow cytometry. Additionally, the antitumor activity in vivo and the effect of the complexes on heart, lung, liver and kidney tissue were studied.

## 2. Experimental

### 2.1. Materials and methods

All reagents and solvents were purchased commercially and used without further purification unless otherwise noted. Ultrapure MilliQ water was used in all experiments. RPMI 1640 were purchased from Sigma. 1,10-Phenanthroline was obtained from the Guangzhou Chemical Reagent Factory. The cancer cell lines of BEL-7402 (human hepatocellular carcinoma), SGC-7901 (human gastric adenocarcinoma), A549 (human lung carcinoma), HepG2 (human hepatocellular carcinoma) and normal NIH3T3 cells (human liver cells) were purchased from the American Type Culture Collection. MitoTracker ® Deep Red FM (150 nM, $\lambda_{ex}$ = 575 nm, $\lambda_{em}$ = 600 nm), 2′,7′-dichlorodihydro-fluorescein diacetate (DCHF-DA, 10 μM, $\lambda_{ex}$ = 488 nm, $\lambda_{em}$ = 525 nm), Fluo-3 AM (Molecular Probes, Eugene, OR, 2.5 μM, $\lambda_{ex}$ = 488 nm, $\lambda_{em}$ = 525 nm), 5,5′,6,6′-tetrachloro-1,1′,3,3′-tetraethylbenzimidazolylcarbocyanine iodide (JC-1, $\lambda_{ex}$ = 514 nm, $\lambda_{em}$ = 529 nm). $IrCl_3{\cdot}3H_2O$ was purchased from the Kunming Institution of Precious Metals. Microanalysis (C, H, and N) was carried out with a PerkinElmer 240Q elemental analyzer. Electrospray ionization mass spectra (ESI-MS) were recorded on a LCQ system (Finnigan MAT, USA) using acetonitrile as the mobile phase. The spray voltage, tube lens offset, capillary voltage and capillary temperature were set at 4.50 kV, 30.00 V, 23.00 V and 200 °C, respectively, and the quoted *m/z* values are for the major peaks in the isotope distribution. $^1H$ NMR and $^{13}C$ NMR spectra were recorded on a Varian-500 spectrometer with DMSO-$d_6$ as a solvent and tetramethylsilane (TMS) as an internal standard at 500 MHz at room temperature.

### 2.2. Synthesis of complexes

#### 2.2.1. Synthesis of $[Ir(ppy)_2(adppz)]PF_6$ (1)

A mixture of cis-$[Ir(ppy)_2Cl]_2$ [35] (0.15 g, 0.14 mmol) and adppz (0.149 g, 0.50 mmol) [33] in a mixture of 42 mL dichloromethane and methanol ($V_{CH2Cl2}$:$V_{CH3OH}$ = 2:1) was refluxed under argon for 6 h to give a clear yellow solution. Upon cooling, a yellow precipitate was obtained by dropwise addition of saturated aqueous $NH_4PF_6$ solution with stirring at room temperature for 2 h. The solvent was removed and the crude product was purified by column chromatography on neutral alumina with a mixture of $CH_2Cl_2$-acetone (1:3, *v*/v) as eluent. The red band was collected. The solvent was removed under reduced pressure and a red powder was obtained. Yield: 79%. Anal. Calc for $C_{40}H_{27}N_7IrPF_6$: C, 50.95; H, 2.89; N, 10.40%. Found: C, 50.83, H, 2.76, N, 10.55%. $^1H$ NMR (DMSO-$d_6$, 500 MHz): $\delta$ 9.40 (d, 2H, *J* = 8.5 Hz), 8.28 (dd, 2H, *J* = 8.0, *J* = 8.5 Hz), 8.21 (d, 2H, *J* = 5.0 Hz), 8.04–7.86 (m, 6H), 7.67 (d, 1H, *J* = 5.5 Hz), 7.63 (d, 2H, *J* = 6.0 Hz), 7.55 (d, 1H, *J* = 7.0 Hz), 7.08–7.01 (m, 4H), 6.96 (t, 2H, *J* = 6.5 Hz), 6.84 (s, 1H), 6.29 (dd, 2H, *J* = 7.5, *J* = 7.5 Hz), 4.56 (s, 2H). $^{13}C$ NMR (125 MHz, DMSO-$d_6$): 166.91, 166.88, 153.01, 151.27, 150.21, 150.00, 149.97, 149.54, 148.91, 147.47, 145.24, 144.09, 139.42, 138.85, 137.73, 134.79, 134.09, 133.79, 131.26, 131.15, 130.63, 130.51, 130.36, 128.06, 127.88, 126.66, 125.15, 123.90, 122.53, 120.03. ESI-MS ($CH_3CN$): *m/z* 796.2 ($[M\text{-}PF_6]^+$).

#### 2.2.2. Synthesis of $[Ir(bzq)_2(adppz)]PF_6$ (2)

This complex was synthesized in a manner identical to **1**, with $[Ir(bzq)_2Cl]_2$ [35] in place of $[Ir(ppy)_2Cl]_2$. Yield: 71%. Anal. Calcd. for $C_{44}H_{27}N_7IrPF_6$: C, 53.33; H, 2.75; N, 9.89%. Found: C, 53.44, H, 2.83, N, 9.96%. $^1H$ NMR (500 MHz, DMSO-$d_6$): $\delta$ 9.31 (d, 2H, *J* = 8.0 Hz), 8.52 (dd, 2H, *J* = 8.0, *J* = 8.0 Hz), 8.25 (dd, 4H, *J* = 8.0, *J* = 8.0 Hz), 8.01 (d, 4H, *J* = 6.0 Hz), 7.88 (d, 4H, *J* = 8.5 Hz), 7.56 (d, 4H, *J* = 7.0 Hz), 7.21 (t, 2H, *J* = 7.5 Hz), 6.85 (s, 1H), 6.31 (dd, 2H, *J* = 6.5, *J* = 7.0 Hz), 3.46 (s, 2H), $^{13}C$ NMR (DMSO-$d_6$, 125 MHz): 156.36, 152.96, 151.75, 150.68, 149.30, 149.26, 149.19, 147.87, 146.75, 145.52, 145.21, 140.38, 139.42, 137.69, 137.64, 136.86, 136.16, 134.79, 134.08, 133.79, 133.26, 132.56, 131.09, 130.80, 130.58, 130.47, 129.77, 129.54, 128.57, 128.36, 128.04, 127.98, 127.79, 127.49, 127.12, 126.74, 126.59, 126.05, 125.67, 124.27, 123.93, 123.78, 122.79, 122.39. ESI-MS ($CH_3CN$): *m/z* 844.2 ($[M\text{–}PF_6]^+$).

#### 2.2.3. Synthesis of $[Ir(piq)_2(adppz)]PF_6$ (3)

This complex was synthesized in a manner identical to **1**, with $[Ir(piq)_2Cl]_2$ [35] in place of $[Ir(ppy)_2Cl]_2$. Yield: 72%. Anal. Calc for $C_{48}H_{31}N_7IrPF_6$: C, 55.28; H, 3.00; N, 9.40%. Found: C, 55.45, H, 2.87, N, 9.51%. $^1H$ NMR (500 MHz, DMSO-$d_6$): $\delta$ 9.35 (d, 2H, *J* = 8.0 Hz) , 9.02 (d, 2H, *J* = 5.0 Hz), 8.41 (d, 2H, *J* = 5.5 Hz), 8.08–7.93 (m, 6H), 7.86 (dd, 6H, *J* = 7.0, *J* = 7.0 Hz), 7.59–7.46 (m, 4H), 7.17 (t, 2H,

$J$ = 7.5 Hz), 7.04 (d, 1H, $J$ = 7.0 Hz), 6.96 (t, 2H, $J$ = 7.5 Hz), 6.84 (s, 2H), 3.42 (s, 2H). 167.91, 167.86, 153.39, 153.00, 151.21, 150.16, 148.72, 147.26, 145.43, 145.21, 141.17, 139.35, 137.73, 136.63, 134.73, 134.02, 133.79, 132.15, 131.73, 130.74, 130.49, 129.48, 128.03, 127.76, 126.67, 126.51, 125.61, 122.51, 122.25. ESI-MS ($CH_3CN$): $m/z$ 898.2 ($[M\text{-}PF_6]^+$).

### 2.3. Colony formation

A549 cells were inoculated into a six-well plate to make the cell density of each well of $5 \times 10^4$. After 24 h, complexes **1** (4.2 μM), **2** (4.8 μM) and **3** (1.2 μM) were added into the wells. After A549 cells were exposed to the complexes for 24 h, the medium was discarded and new medium was added, the cell colonies were grown for 10 days, then the medium was discarded, the cells were washed with phosphate buffered saline (PBS) three times and fixed with paraformaldehyde solution for 20 min, and then stained with crystal violet (0.1%, *w/v*) for 20 mins, the cells were imaged under light microscope.

### 2.4. Cytotoxicity assay in vitro

MTT assay procedures were used to evaluate the cytotoxic activity of the complexes against the above cell lines [22,36]. After the cells were treated by the different concentrations of the complexes (dissolved in DMSO and final concentration of DMSO is 0.05%, *v*/v) for 48 h, the stock MTT dye solution (20 μL, 5 mg·mL$^{-1}$) was added to each well. After 4 h, buffer (100 μL) containing dimethylformamide (50%) and sodium dodecyl sulfate (20%) was added to solubilize the MTT formazan. The optical density of each well was measured with a microplate spectrophotometer at a wavelength of 490 nm. Each experiment was repeated at least three times to obtain mean values.

### 2.5. Location of the complexes at the lysosomes

A549 cells were incubated with 0.6 μM of complexes **1–3** for 3 h and stained with LysoTracker Red (150 nM) at 37 °C for 0.5 h. The wells were washed three times with ice-cold PBS, then the cells were imaged under a fluorescence microscope.

### 2.6. Detection of lysosomal membrane permeabilition

A549 cells were exposed to 0.6 μM of complexes **1–3** for 24 h and further co-incubated with AO (1 μg mL$^{-1}$) at 37 °C for 0.5 h. Upon completion of the incubation, the wells were washed three times with ice-cold PBS. After discarding the culture medium, the cells were imaged under a fluorescence microscope.

### 2.7. Reactive oxygen species (ROS) detection

A549 cells were cultured in RPMI (Roswell Park Memorial Institute) 1640 medium supplemented with 10% FBS (Fetal Bovine Serum) and incubated at 37 °C in 5% $CO_2$. The cells were treated with different concentrations of the complexes (DMSO concentration, 0.05% *v*/v) for 24 h. The fluorescent dye 2′,7′-dichlorodihydro-fluorescein diacetate (DCHF-DA, 10 μM) was added for 30 min and the cells were washed twice with cold PBS–EDTA. The cells were collected by trypsinization and centrifugation at 1500 rpm for 5 min. The DCF fluorescence intensity was determined by flow cytometry.

### 2.8. Location of the complexes at endoplasmic reticulum and measurement of intracellular $Ca^{2+}$ levels

#### 2.8.1. Location of the complexes at endoplasmic reticulum

Appropriate A549 cells were placed in a 12-well microassay plate, placed in a 37 °C, 5% $CO_2$ incubator, and 1.2 μM of complexes **1–3** were added to the well for 3 h, then ER-Tracker Red (667 nM) was incubated at 37 °C for 0.5 h and then incubated with DAPI (100 μM) for 0.5 h at 37 °C. After the incubation was completed, the wells were washed three times with HBSS (Hank's Balanced Salt Solution) with $Ca^{2+}$ & $Mg^{2+}$ and the cells were imaged under a fluorescence microscope.

#### 2.8.2. Measurement of intracellular $Ca^{2+}$ levels

A549 cells were seeded into chamber slides in 12-well plates and incubated for 24 h. The cells were treated with 0.6 μM of the complexes (DMSO concentration, 0.05% *v*/v) for 24 h. The cells were washed with PBS twice. Then the cells were stained with Fluo-3 AM (Molecular Probes, Eugene, OR, 2.5 μM) for 30 min and washed with PBS twice. After this, the cells were stained with DAPI (2-(4-amidinophenyl)-6-indolecarbamidine dihydrochloride, 10 μg mL$^{-1}$) for 30 min and washed with PBS twice. The cells were imaged and analyzed under the Molecular Devices.

### 2.9. Location assay of the complexes in the mitochondria

A549 cells were incubated with 3.0 μM of the complexes for 2 h and further co-incubated with MitoTracker ® Deep Red FM (150 nM) at 37 °C for 0.5 h. Upon completion of the incubation, the wells were washed three times with ice-cold PBS. Then the cells were imaged under a fluorescence microscope.

### 2.10. Mitochondrial membrane potential assays

A549 cells were treated with different concentrations of the complexes for 24 h and then washed three times with cold PBS. The cells were detached with trypsin–EDTA (Ethylene Diamine Tetraacetie Acid) solution. The collected cells were incubated for 20 min with 1 μg mL$^{-1}$ of JC-1 (5,5′,6,6′-tetrachloro-1,1′,3,3′-tetraethylimidacarbocyanine iodide). The cells were then immediately centrifuged to remove the supernatant. The ratio of red/green fluorescence intensity was determined by flow cytometry.

### 2.11. Determination of ATP content

A549 cells ($5 \times 10^5$) were plated in a 6-well plate. 3.2, 4.8 and 1.2 μM of complexes **1**, **2** and **3** were incubated for 24 h. The cells were lysed and collected by centrifugation, and the supernatant was extracted for subsequent determination. The ATP content of the sample was determined by an enhanced ATP (Adenosine triphosphate) detection kit (Beyotime, China). The concentration of ATP was calculated.

### 2.12. Release of cytochrome c

A549 cells were treated with 0.6 μM of the complexes (DMSO concentration, 0.05% *v*/v) for 24 h. The cells were washed twice with PBS and the cells were fixed with stationary liquid overnight at 4 °C. Then the cells were incubated with confining liquid for 1 h, washed with PBST (Phosphate Buffer Saline, Tween-20) three times. Finally, the cells were incubated with primary antibody of human cytochrome *c* for 24 h. The cells were incubated with fluorescein conjugated anti-mouse secondary antibody and stained with DAPI.

### 2.13. Comet assay

DNA damage was investigated by means of comet assay. A549 cells in culture medium were incubated with 1.2 μM of complexes **1–3** for 24 h at 37 °C. The cells were harvested. A total of 100 μL of 0.5% normal agarose in PBS was dropped gently onto a fully frosted microslide, covered immediately with a coverslip, and then placed at 4 °C for 10 min. The coverslip was removed after the gel had set. 50 μL of the cell suspension (200 cells per μL) was mixed with 50 μL of 1% low melting agarose preserved at 37 °C. A total of 100 μL of this mixture was applied quickly on top of the gel, coated over the microslide, covered

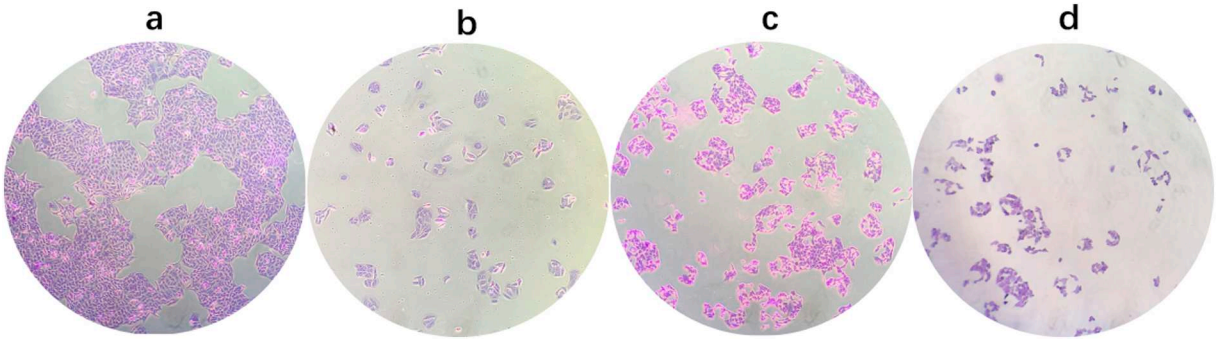


**Fig. 1.** Inhibition of A549 (a) cell colonies induced by $IC_{50}$ values of complexes **1** (b), **2** (c) and **3** (d) for 10 days.

**Table 1**
$IC_{50}$ (μM) values of the complexes toward the selected cancer cell lines.

| Complex | A549 | BEL-7402 | SGC-7901 | HepG2 | NIH 3 T3 |
|---|---|---|---|---|---|
| adppz | 25.6 ± 2.0 | > 200 | 61.1 ± 5.9 | > 200 | > 200 |
| 1 | 3.2 ± 0.4 | 7.4 ± 1.6 | 4.9 ± 0.6 | 15.4 ± 2.2 | 12.8 ± 1.6 |
| 2 | 4.8 ± 0.5 | 4.6 ± 1.5 | 1.3 ± 0.04 | 5.7 ± 0.8 | 11.4 ± 2.0 |
| 3 | 1.2 ± 0.2 | 4.9 ± 1.3 | 2.4 ± 0.5 | 17.3 ± 2.7 | 5.1 ± 0.7 |
| cisplatin | 7.5 ± 1.3 | 10.8 ± 1.6 | 3.6 ± 0.5 | 12.5 ± 1.5 | nd |

nd: not determination.

immediately with a coverslip, and then placed at 4 °C for 10 min. The coverslip was again removed after the gel had set. A third coating of 50 μL of 0.5% low melting agarose was placed on the gel and allowed to set at 4 °C for 15 min. After solidification of the agarose, the coverslips were removed, and the slides were immersed in an ice-cold lysis solution (2.5 M NaCl, 100 mM EDTA, 10 mM Tris, 90 mM sodium sarcosinate, NaOH, pH 10, 1% Triton X-100 and 10% DMSO) and placed in a refrigerator at 4 °C for 2 h. All of the above operations were performed under low lighting conditions to avoid additional DNA damage. The slides, after removal from the lysis solution, were placed horizontally in an electrophoresis chamber. The reservoirs were filled with an electrophoresis buffer (300 mM NaOH, 1.2 mM EDTA) until the slides were just immersed in it, and the DNA was allowed to unwind for 30 min in electrophoresis solution. Then the electrophoresis was carried out at 25 V and 300 mA for 20 min. After electrophoresis, the slides were removed, washed thrice with a neutralization buffer (400 mM Tris, HCl, pH 7.5). The cells were stained with 20 μL of EB (Ethidium Bromide, 20 μg $mL^{-1}$) in the dark for 20 min. The slides were washed in chilled distilled water for 10 min to neutralize the excess alkali, air-dried and scored for comets under a fluorescent microscopy.

### 2.14. Apoptosis assays by AO/EB staining and flow cytometry

A549 cells were cultured in RPMI 1640 containing 10% of FBS and incubated at 37 °C in 5% $CO_2$ for 24 h, the cells were treated with the complexes (0.6 μM) (DMSO concentration, 0.05% *v*/v) for 24 h. The cells were washed with ice-cold PBS, and fixed with formalin (4%, *w*/*v*). The cell nuclei were counterstained with acridine orange (AO) and ethidium bromide (EB) (AO: 100 μg $mL^{-1}$, EB: 100 μg$mL^{-1}$) for 10 min. Then the cells were observed and imaged under a fluorescence microscope (Nikon, Yokohama, Japan) with excitation at 350 nm and emission at 460 nm.

After chemical treatment, A549 cells ($1 \times 10^6$) were harvested, washed with PBS, fixed with 70% ethanol, and finally maintained at 4 °C for 24 h. The pellets were stained with 50 μg $mL^{-1}$ PI (propidium iodide) and 1 mg $mL^{-1}$ Annexin V in PBS on ice in the dark for 15 min. The fluorescence emission was measured at 530 nm (excitation at 488 nm) with a FACS Calibur flow cytometry (Beckman Dickinson & Co., Franklin Lakes, NJ). A minimum of 10,000 cells were analyzed per sample.

### 2.15. Matrigel invasion assay

A549 cells ($4 \times 10^4$) in serum free medium containing different concentrations of the complex were seeded into the top chamber of the two-chamber Matrigel system. RPMI 1640 medium (20% FBS) was added into the lower chamber. The cells were allowed to invade for 24 h. After incubation, non-invading cells were removed from the upper surface and cells on the lower surface were fixed with 4% paraformaldehyde and stained with 0.1% crystal violet. The mean values from three independent assays were calculated.

### 2.16. Cell cycle arrest by flow cytometry

A549 cells were seeded into six-well plates (Costar, Corning Corp, New York) at a density of $2 \times 10^5$ cells per well and incubated for 24 h. The cells were cultured in RPMI 1640 medium supplemented with 10% FBS and incubated at 37 °C in 5% $CO_2$. The cells were incubated with the complexes (1.2 μM) (DMSO concentration, 0.05% *v*/v) for 24 h, the cell layer was trypsinized and washed with cold PBS and fixed with 70% ethanol. 20 μL of RNAse (0.2 mg $mL^{-1}$) and 20 μL of propidium iodide (0.02 mg $mL^{-1}$) were added to the cell suspensions and they were incubated at 37 °C for 30 min. Then the cells were analyzed with a FACS Calibur flow cytometer.

### 2.17. Fluorescence spectroscopy

All BSA (Bovine Serum Albumin) solutions were prepared in the 5 mM Tris–HCl/10 mM NaCl buffer (pH = 7.4). The BSA stock solution was stored at 4 °C in the dark and used within 2 h. Quenching of BSA was performed by taking a fixed concentration of the BSA solution ($5 \times 10^{-3}$ M BSA) with increasing amounts of the iridium(III) complexes. The fluorescence spectra were recorded at an excitation wavelength of 280 nm and emission was observed at room temperature after each addition of the quencher and results were analyzed.

### 2.18. Expression of caspases and Bcl-2 family proteins induced by the complexes

A549 cells were incubated with 1.2 μM of the complexes in the presence of 10% FBS for 24 h. The cells were harvested in lysis buffer. After sonication, the cells were centrifuged for 20 min at 13000 *g*. The protein concentration of the supernatant was determined by BCA (bicinchoninic acid) assay. Sodium dodecyl sulfate–polyacrylamide gel electrophoresis was performed by loading equal amounts of protein per lane. The gels were then transferred to poly(vinylidene difluoride) membranes (Millipore) and blocked with 5% non-fat milk in TBST (20 mM Tris–HCl, 150 mM NaCl, 0.05% Tween 20, pH 8.0) buffer for 1 h. Then the membranes were incubated with primary antibodies at 1:5000 dilutions in 5% non-fat milk overnight at 4 °C, and washed four times with TBST for a total of 30 min. After this, the membranes were incubated with secondary antibodies conjugated with horseradish

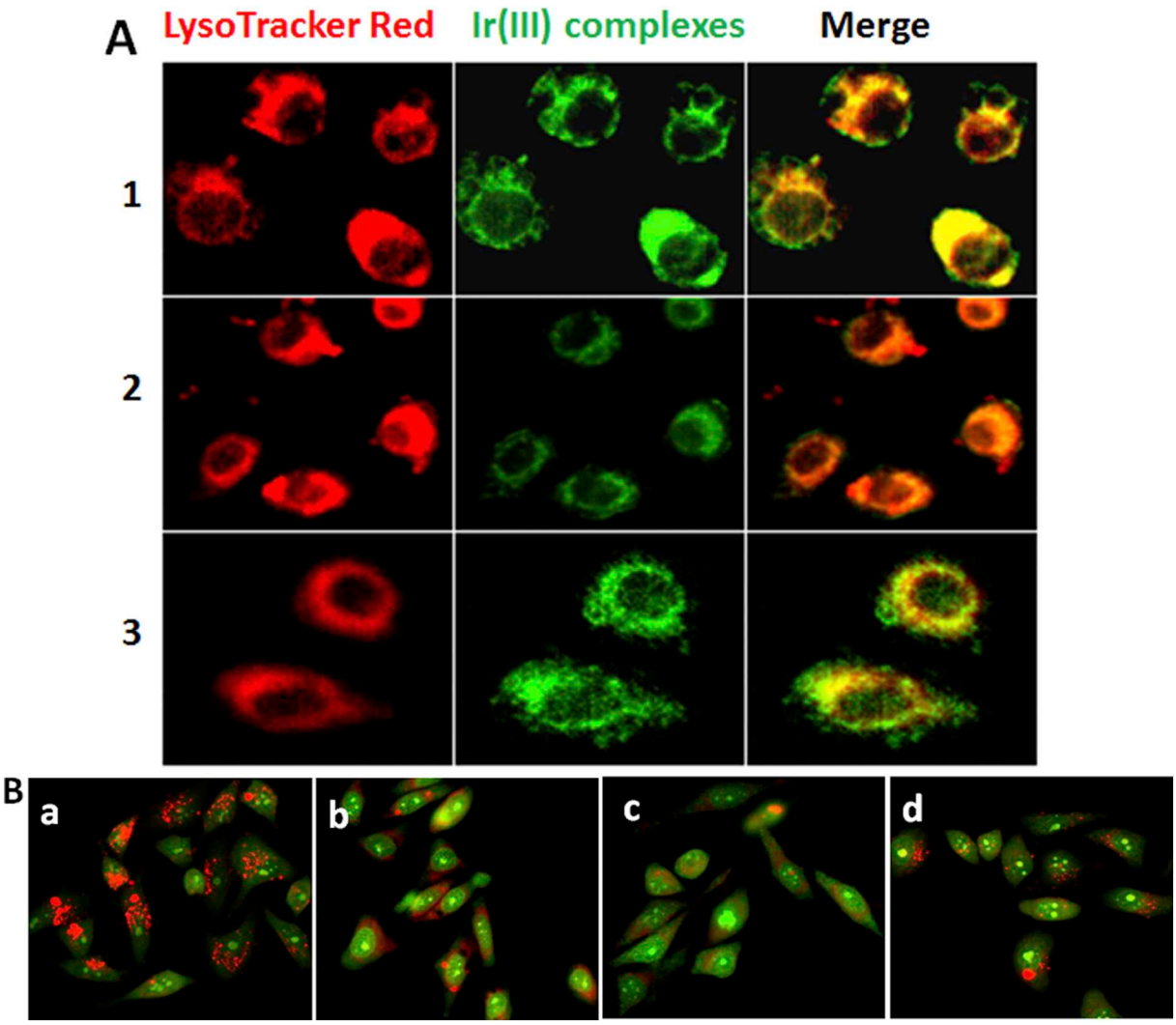


**Fig. 2.** (A) Location of the complexes at the lysosomes after A549 cells were treated with 1.2 μM of complexes **1**–**3** for 3 h. (B) Assays of lysosomal permeabilization after A549 cells (a) were exposed to 1.2 μM of complexes **1** (b), **2** (c) and **3** (d) for 6 h and the cells were stained with AO.

peroxidase (diluted at a ratio of 1:5000) for 1 h at room temperature and then washed four times with TBST. The blots were visualized using Amersham ECL Plus western blotting detection reagents according to the manufacturer's instructions. β-actin was used as internal control.

### 2.19. Evaluation of antitumor activity in vivo

Mice with human tumor xenografts were provided by the Laboratory Animal Center of Sun Yat-Sen University (Guangzhou). All animal procedures were approved by the Animal Ethical Committee of Guangdong Pharmaceutical University. Different doses of 1.14 and 2.28 mg/kg of complex **3** were injected intraperitoneally into mice of different group (each group contained 6 mice) once a day for eight consecutive days beginning 24 h after inoculation. This dose was the maximum tolerated dose based on our preliminary studies. Cisplatin (2 mg/kg) was used as a positive control. The mice in the control were injected with the vehicle. Compounds were administered by exact body weight, with the injection volume being not > 0.2 mL. The weights of the animals were recorded every 1 day. All animals were sacrificed on the eighteenth days after tumor inoculation, and the tumors were excised and weighed. The inhibitory rate was calculated as follow:

$$[(C - T)/C] \times 100\%$$

T is the average tumor weight of the treated group and C is the average tumor weight of the negative control group [37].

### 2.20. Data analysis

All data were expressed as mean ± SD. Statistical significance was evaluated using *t*-tests. Differences were considered to be significant when the $^*P$ value was $< 0.05$.

## 3. Results and discussion

### 3.1. Inhibition of colonies

One of the characteristics of tumor cells is that they can migrate and proliferate in new sites and form secondary tumors. Therefore, studying colony formation is an important way to study tumor cell metastasis. We studied the inhibition of A549 cell colonies after A549 cells were treated with the complexes **1** (3.2 μM), **2** (4.8 μM) and **3** (1.2 μM) for 10 days. As shown in Fig. 1, the cell colonies treated with the complexes were obviously inhibited compared with the control group. Hence, the complexes can effectively inhibit the cells to form colonies.

### 3.2. Cytotoxicity in vitro studies

The cytotoxic activity in vitro of complexes **1**, **2**, and **3** against

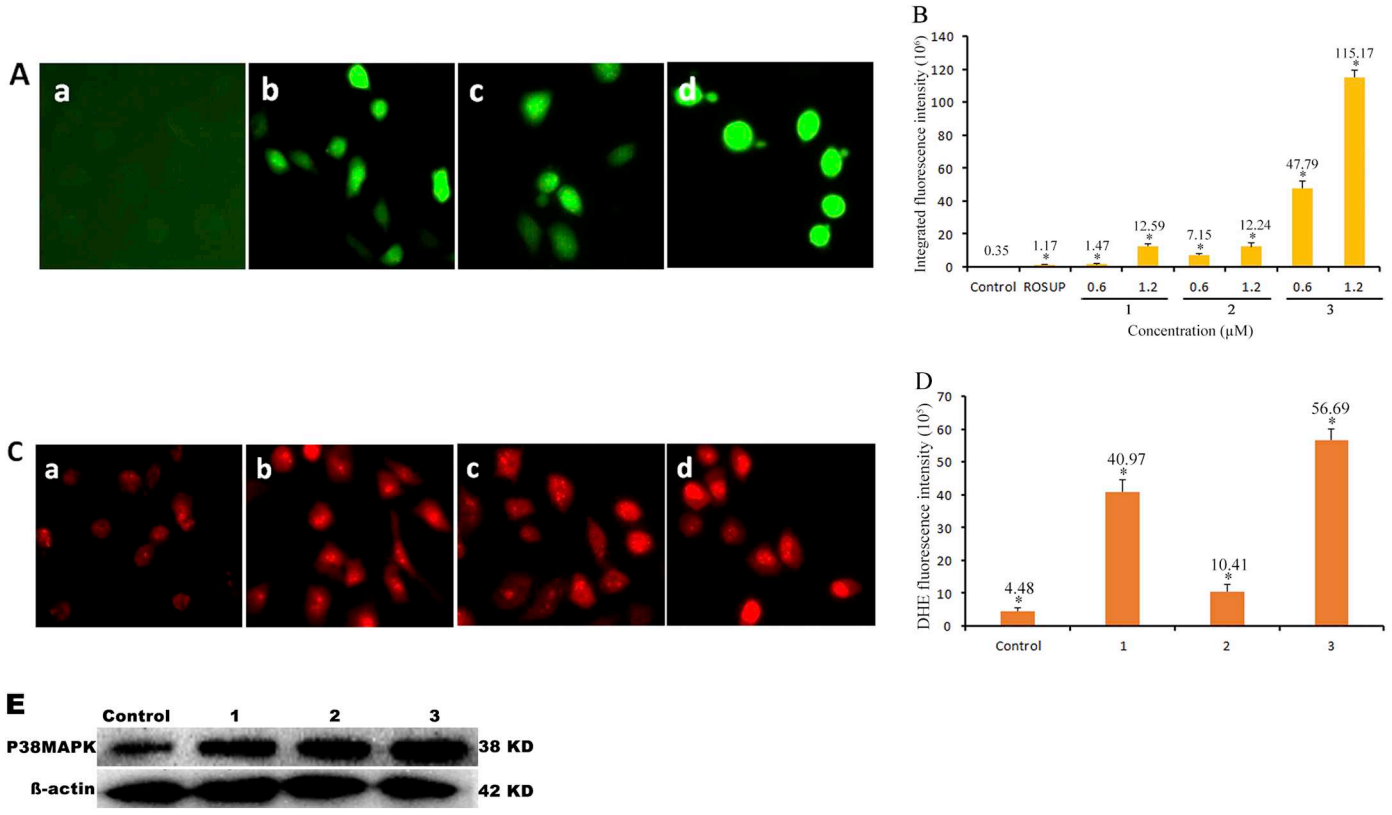


**Fig. 3.** (A) Intracellular ROS was detected in A549 cells (a) exposure to 0.6 μM of **1.** (b), **2** (c) and **3** (d) for 24 h. (B) The DCF fluorescent intensity was determined after A549 cells were treated with ROSUP (positive control) and different concentration of the complexes for 24 h. (C) The superoxide anion level was assayed after 24 h of A549 cells (a) exposure to 0.6 μM of **1** (b), **2** (c) and **3** (d) and the cells were stained with DHE. DHE fluorescent intensity was determined (D). (E) The expression of p38MAPK induced by $IC_{50}$ values of complexes **1**, **2** and **3** for 24 h. $^*P < 0.05$ represents significant differences compared with control.

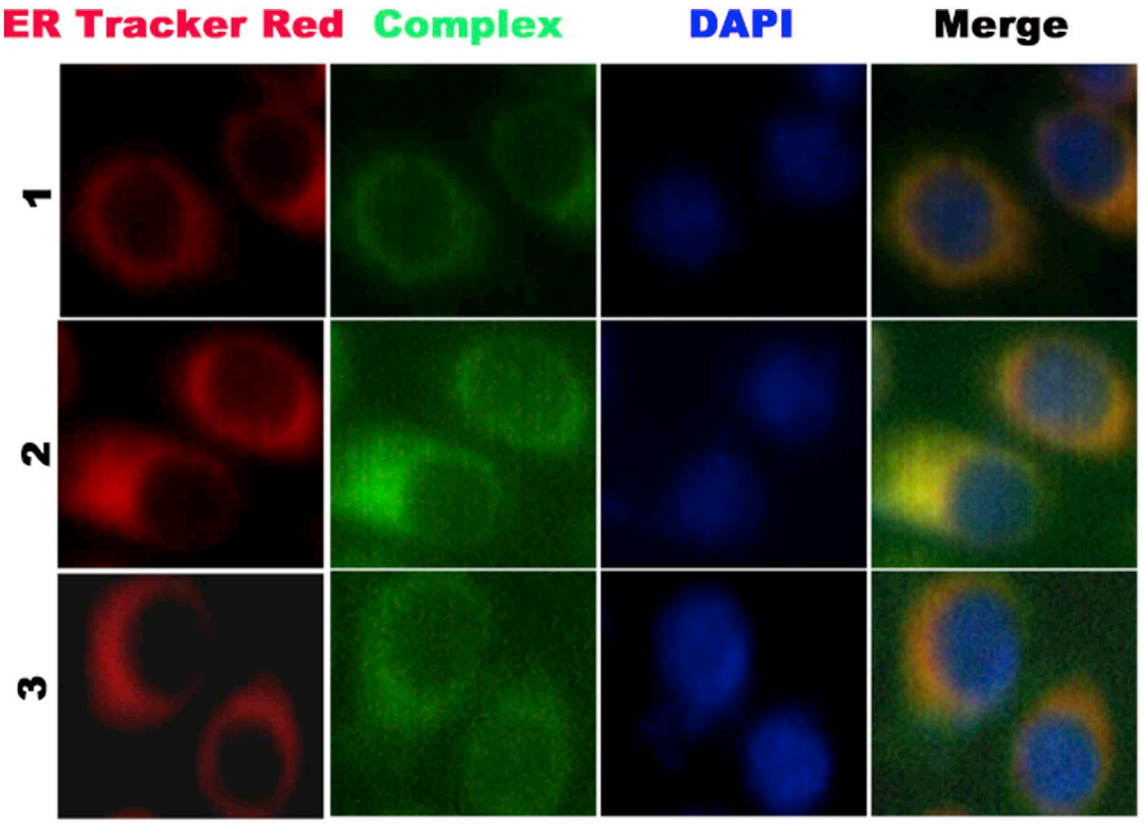


**Fig. 4.** Location of the complexes at endoplasmic reticulum after A549 cells were exposed to 1.2 μM of the complexes for 3 h.

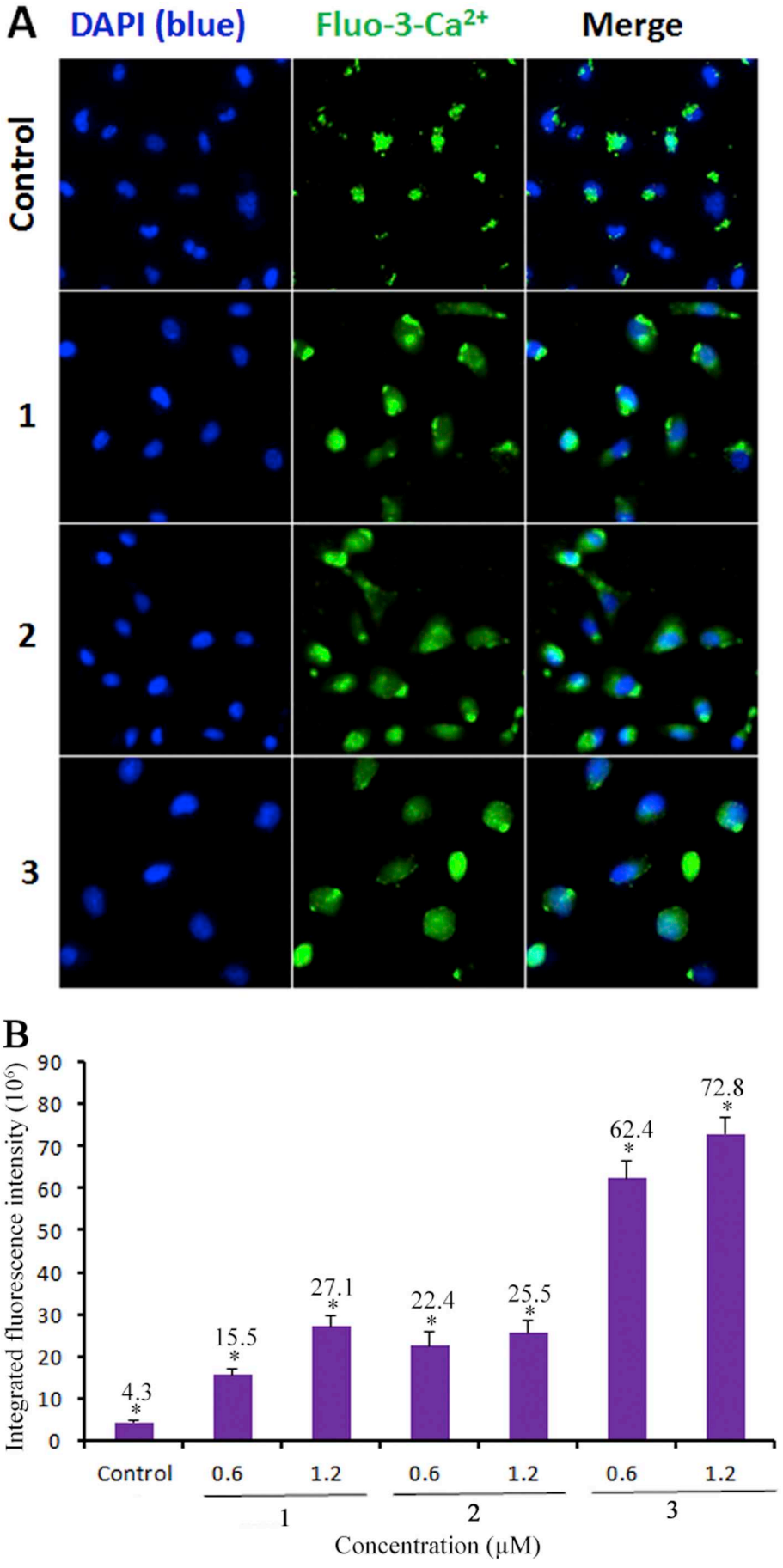


*(caption on next page)*

**Fig. 5.** (A) Intracellular $Ca^{2+}$ levels were assayed after A549 cells were exposed to 0.6 μM of **1**, **2** and **3** for 24 h. (B) The integrated fluorescent intensity/cell was determined after A549 cells were treated with different concentrations of the complexes for 24 h. *$P < 0.05$ represents significant differences compared with control.

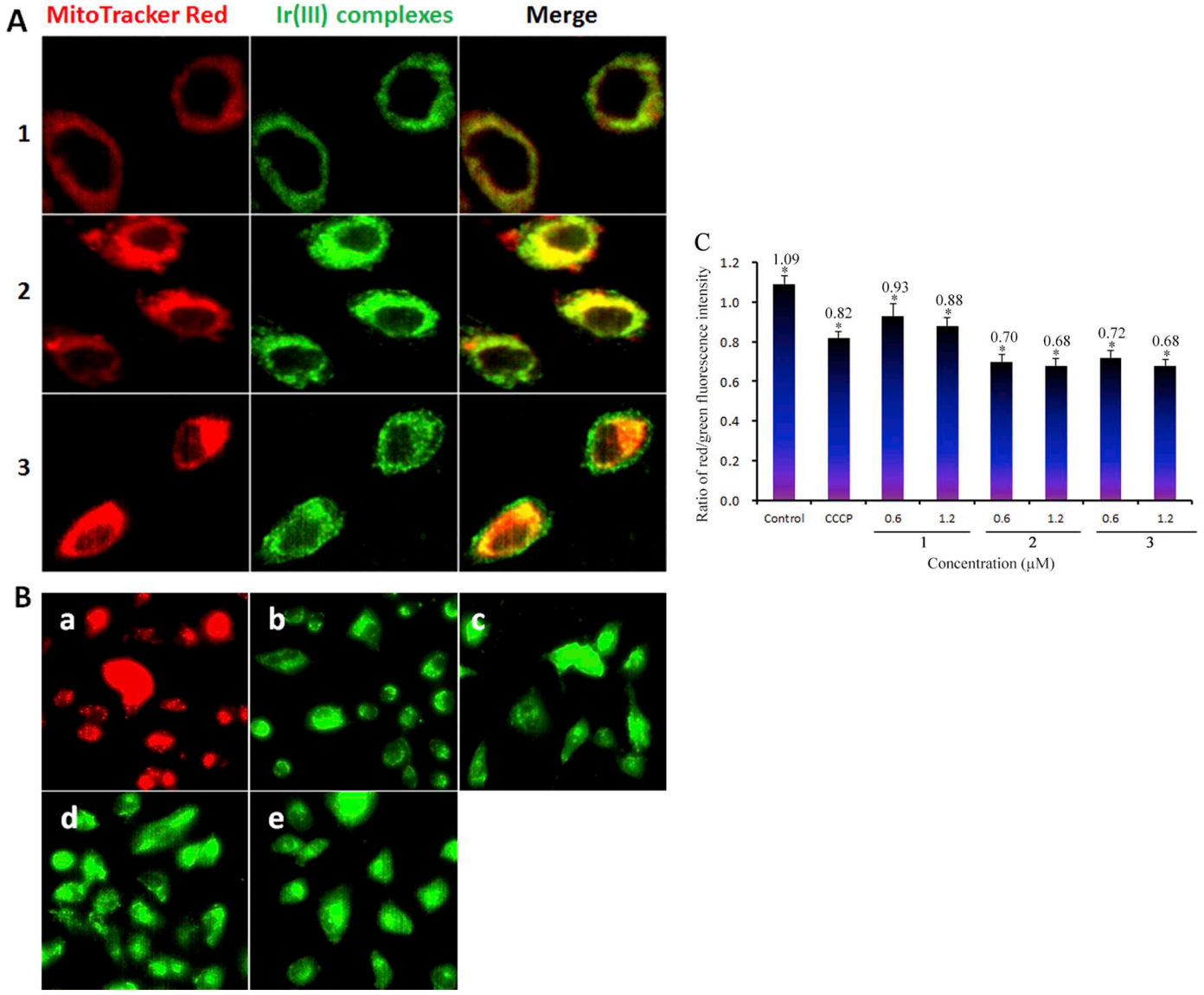


**Fig. 6.** (A) Location assays of the complexes in the mitochondria. (B) The mitochondrial membrane potential was determined under fluorescent microscope while A549 cells (a) were treated with CCCP (b, positive control), 1.2 μM of **1** (c), **2** (d) and **3** (e) for 3 h. (C) The ratio of red/green fluorescence intensity was determined while A549 cells were incubated with different concentrations of the complexes for 24 h. *$P < 0.05$ represents significant differences compared with control. (For interpretation of the references to colour in this figure legend, the reader is referred to the web version of this article.)

**Table 2**
ATP amount in the cells.

| Complex | ATP amount (μM) |
|---|---|
| Control | 0.741 |
| 1 | 0.738 |
| 2 | 0.658 |
| 3 | 0.622 |

cancer A549, BEL-7402, SGC-7901, HepG2 and normal NIH3T3 cells was evaluated by MTT methods, and cisplatin was used as a positive control. The data are expressed as $IC_{50}$ values (50% inhibitory concentration), which is defined as the compound concentration that reduces cell proliferation by 50% and are shown in Table 1. As expectation, ligand adppz shows low against A549 and SGC-7901 cells, and no cytotoxic activity against cancer BEL-7402, HepG2 and normal NIH 3 T3 cells. Complexes **1–3** reveal strong inhibitory effect on the cell growth toward the selected cancer cells, their $IC_{50}$ values range from 1.2 ± 0.2 to 17.3 ± 2.7 μM. In particular, complexes **1**, **2** and **3** shows high ability to inhibit the cell growth in A549 and SGC-7901 cells. Among the three complexes, complexes **3** and **2** display the highest anticancer activity against A549 and SGC-7901 cells, with a low $IC_{50}$ value of 1.2 ± 0.2 and 1.3 ± 0.04 μM, respectively. Hence, different complex exhibits different anticancer effect on the different cancer cells. Although complexes **1–3** contain the same main ligand adppz, different ancillary ligands ppy for **1**, bzq for **2** and piq for **3** result in different anticancer activity. Comparing the $IC_{50}$ values of the complexes **1–3** with $[Ir(L)_2(ndppz)](PF_6)$ (L = ppy, **Ir-1**; bzq, **Ir-2**; piq, **Ir-3**)

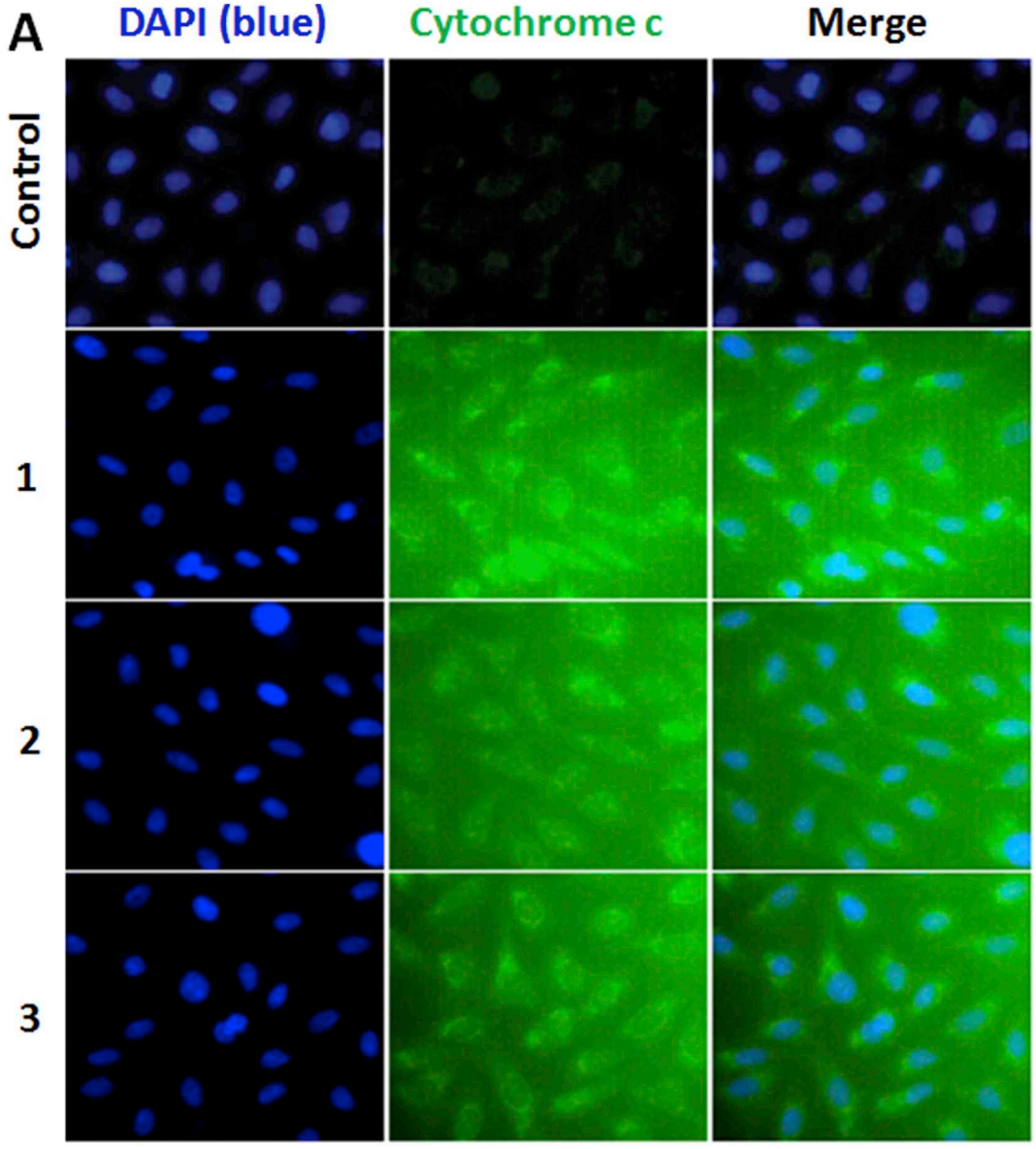


*(caption on next page)*

**Fig. 7.** (A) The release of cytochrome *c* was assayed after A549 cells (a) were exposed to 0.6 μM of **1**, **2** and **3** for 24 h. (B) The integrated fluorescent intensity/cell was determined after the treatment of A549 cells with different concentration of the complexes for 24 h. $*P < 0.05$ represents significant differences compared with control.

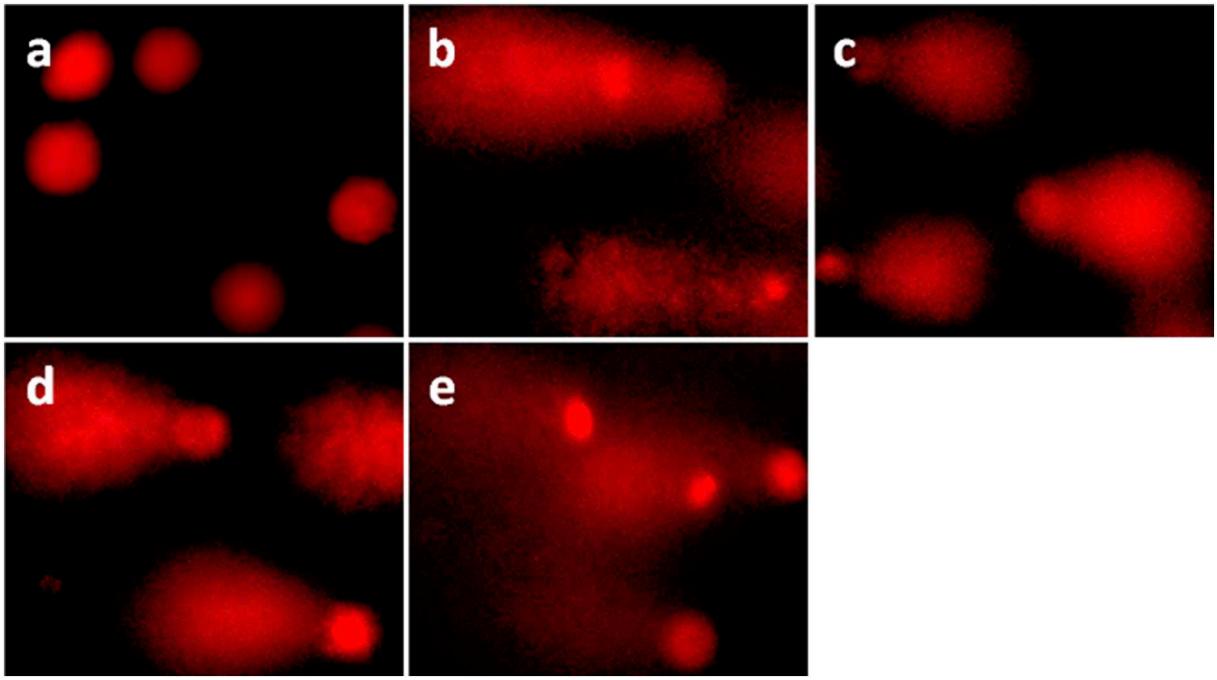


**Fig. 8.** Comet assay of A549 (a) exposure to $H_2O_2$ (positive control, 100 μM, b) and 1.2 μM of **1** (c), **2** (d) and **3** (e) for 24 h.

[34], complexes **1–3** reveal comparable cytotoxic activity with **Ir-1**, **Ir-2** and **Ir-3** toward A549 and BEL-7402 cells. However, complexes **1** ($IC_{50}$ = 4.9 ± 0.6 μM) and **3** ($IC_{50}$ = 2.4 ± 0.5 μM) show lower cytotoxicity against SGC-7901 cells than **Ir-1** ($IC_{50}$ = 1.8 ± 0.4 μM) and **Ir-3** ($IC_{50}$ = 0.8 ± 0.1 μM). These differences may be attributed to the different amount of cellular uptake. In addition, complexes **1**, **2** and **3** show higher cytotoxicity than cisplatin and comparable with complexes $[Ir(ppy)_2(THPDP)](PF_6)$ (THPDP = 11-(6,7,8,9-tetrahydrophenazin-2-yl)dipyrido[3,2-*a*:2′,3′-*c*]phenazine, $IC_{50}$ = 1.4 ± 0.03 μM) [38] and $[Ir(ppy)_2(BDPIP)(PF_6)$ (BDPIP = 2-(1-benzo[*d*]dioxol-5-yl)propan-2-yl)- 1H-imidazo[4,5-f][1,10]phenanthrene, $IC_{50}$ = 3.6 ± 0.3 μM) [39] toward A549 cells. Regretfully, complexes **1**, **2** and **3** also exhibit cytotoxic activity toward normal NIH 3T3 cells. Because A549 cells are sensitive to **1**, **2** and **3**, this cell line was selected for undergoing the following experiments.

### 3.3. Location of the complexes at the lysosomes and lysosomal permeabilization

Lysosomes are acidic intracellular organelles that are involved in several cellular processes, including receptor degradation, autophagy, apoptosis, post-translational protein maturation, and the extracellular release of active enzymes [40–42]. To evaluate whether the complexes target the lysosomes, the location of the complexes at the lysosomes was investigated. After A549 cells were incubated with 1.2 μM of complexes **1–3** for 3 h, the lysosomes are stained red with LysoTracker red, whereas the complexes emit green fluorescence. The overlap hints that the complexes may enter into the lysosomes (Fig. 2A). The Pearson's colocalization coefficient (PCC) was obtained by analyzing the red and green fluorescent intensity in 50 cells according to literature [43]. The PCC value is 0.3598, which shows a positive correlation. Whereas lysosomal membrane permeabilization (LMP) can release the lysosomal constituents, which further cause cell death. Fig. 2B shows that a decrease in the red and an increase in the green fluorescence was observed, indicating that complexes **1**, **2** and **3** can enhance lysosomal permeabilization, which further confirms that the complexes inhibit the cell growth by targeting the lysosomes.

### 3.4. Intracellular reactive oxygen species (ROS) levels

ROS is defined as containing oxygen free radicals and peroxides, and it is easy to form free radicals related to oxygen metabolism in the body. Accumulation of ROS in cells can induce mitochondrial dysfunction, which promotes the release of cytochrome *c*, and further cause apoptosis. DCFH-DA was used as fluorescence probe to examine intracellular ROS levels. In the presence of intracellular ROS, DCFH-DA is converted into high fluorescence DCF. Fig. 3A shows that the treatment of A549 cells with the complexes, the green fluorescence increases compared with that in the control, which indicates that these complexes can boost intracellular ROS levels. In addition, to compare the efficiency of the complexes **1**, **2** and **3** on the ROS levels, DCF fluorescence intensity was assayed. As shown in Fig. 3B, 1.2 μM of complexes **1**, **2** and **3** give rise to an increasement of 35.97, 34.97 and 329.06 times in the DCF fluorescence than that in the control, respectively. Moreover, complex **3** displays the highest efficiency to generate intracellular ROS levels among these complexes.

ROS include superoxide anion and NO free radical, etc. The superoxide anion $O_2^{\bullet-}$ was also investigated using DHE (Dihydroethidium) as fluorescence probe. As shown in Fig. 3C, the treatment of A549 cells (a) with 0.6 μM of complexes **1** (b), **2** (c) and **3** (d) for 24 h, the red fluorescence intensity increases. The DHE red fluorescence intensity was determined and shown in Fig. 3D, the DHE red fluorescence intensity increases 9.15 for **1**, 2.32 for **2** and 12.65 times for **3** than that in the control. These results further confirm that the complexes can enhance intracellular ROS levels. P38MARK (Mitogen-Activated Protein Kinase) plays an important role in the occurrence, apoptosis and metastasis of tumor cells. p38MARK includes four subtypes of p38α, p38β, p38γ and p38δ, of which p38γ is highly expressed in several human

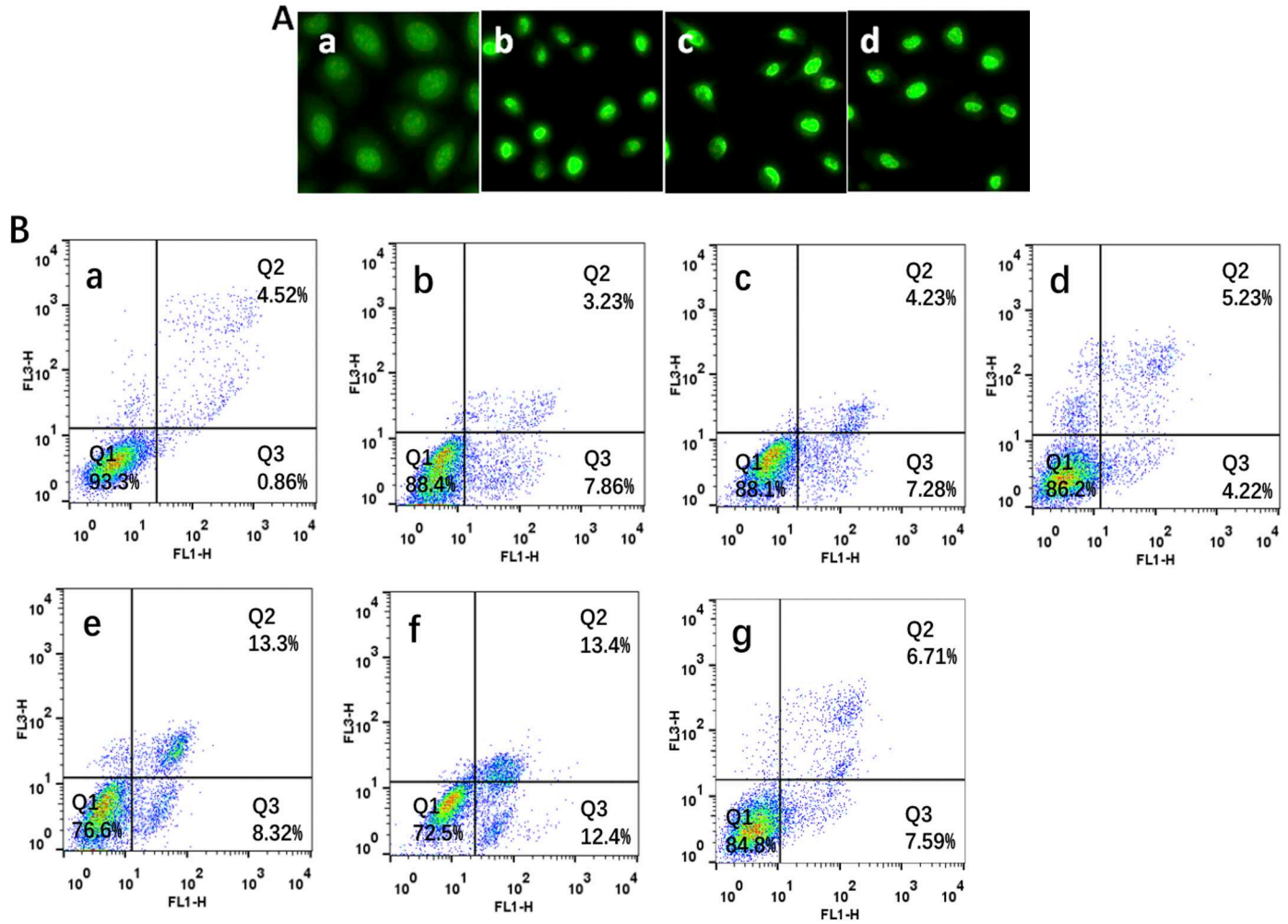


**Fig. 9.** (A) Apoptosis assays of A549 cells (a) exposed to 0.6 μM of **1** (b), **2** (c) and **3** (d) for 24 h and the cell nuclei were stained with AO/EB. (B) The apoptotic percentage of A549 cells (a) were treated with $IC_{50}$ values of **1** (b and e), **2** (c and f), and **3** (d and g) for 24 or 48 h.

tumor cell lines. Western blot analysis was used to detect the expression of p38MARK in the drug-treated group and the blank group. As shown in Fig. 3E, the results showed that the expression of p38MARK in the drug-treated group was significantly increased compared with the blank group, indicating that the complexes **1–3** can regulate the expression of p38MARK, which further suggests that the complexes can induce apoptosis in A549 cells.

### *3.5. Location of the complexes at the endoplasmic reticulum and detection of intracellular $Ca^{2+}$ levels*

It is well known that the endoplasmic reticulum can store $Ca^{2+}$, and $Ca^{2+}$ in the endoplasmic reticulum is released into the cytoplasm, which can activate a calcium channel on the plasma membrane of the cell. $Ca^{2+}$ in the mitochondrial matrix rapidly increases, causing morphological changes, such as swelling and fragmentation, leading to the onset of mitochondria mediated apoptosis. To detect whether the complexes act on the endoplasmic reticulum, A549 cells were treated with 1.2 μM of the complexes for 3 h, the cells were stained with ER Tracker Red and DAPI. As shown in Fig. 4, the endoplasmic reticulum was stained red, the complexes emit green fluorescence, the overlap of the red, green and blue (DAPI) indicates that the complexes act on the endoplasmic reticulum. On the other hand, calcium ion is involved in numerous cellular processes such as fertilization, development, differentiation, and cell death through changing $Ca^{2+}$ cytoplasmic concentrations to control different cellular functions [44–47]. Fluo-3AM (AM = 1-[2-Amino-5-(2,7-dichloro-6-acetoxymethoxy-3-oxo-9-xanthenyl)phenoxy]-2-(2-amino-5-methylphenoxy)ethane-N,N,N′,N′-tetra-acetic acid, tetra(acetoxymethyl)ester) as a fluorescent dye can penetrate cell membranes. The fluorescence of Fluo-3AM is very weak and its fluorescence does not increase with increasing calcium concentration. However, in the cells, Fluo-3AM is converted into Fluo-3, which combines with $Ca^{2+}$ to be transferred into fluorescent Fluo-3-$Ca^{2+}$. After the drug acts on the cells, it causes the continuous open of the $Ca^{2+}$ channels, resulting in changes in mitochondrial and endoplasmic reticulum $Ca^{2+}$ levels, which in turn causes apoptosis [48–50]. As shown in Fig. 5A, a weak green fluorescence was discovered in the control (a). However, 0.6 μM of complexes **1–3** treated A549 cells for 24 h, a number of bright green fluorescence points were observed, which suggested that intracellular $Ca^{2+}$ levels were increased. To quantify the efficiency of the complexes on intracellular $Ca^{2+}$ levels, Fluo-3-$Ca^{2+}$ fluorescence intensity was determined by ImageXpress Micro XLS. See from Fig. 5B, the fluorescence intensity of fluo-3-$Ca^{2+}$ increases 6.30 for **1**, 5.93 for **2** and 15.17 times for **3** than that in the control and abides by the order of complex **3** > **1** > **2** while A549 cells were incubated with 1.2 μM of the complexes. This is in accord with that of cytotoxicity of the complexes toward A549 cells.

### *3.6. Location and mitochondrial membrane potential assays*

The mitochondrion is an essential organelle that plays a crucial role in energy production; its dysfunction would induce irreversible cell

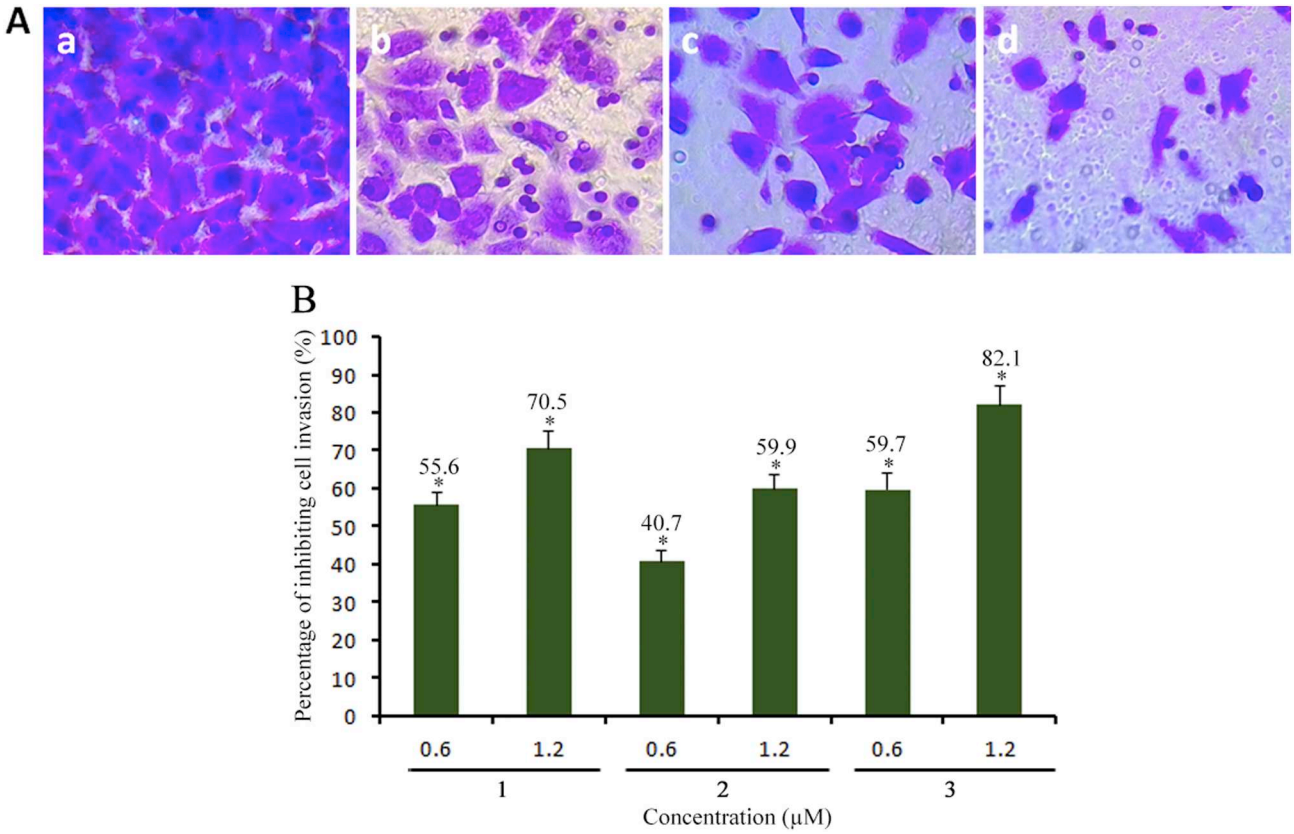


**Fig. 10.** (A) Microscope images of invading A549 cells (a) that have migrated through the Matrigel induced by 0.6 μM of **1** (b), **2** (c) and **3** (d) for 24 h. (B) The percentage of inhibiting cell invasion of A549 cells induced by different concentration of the complexes for 24 h. $^*P < 0.05$ represents significant differences compared with control.

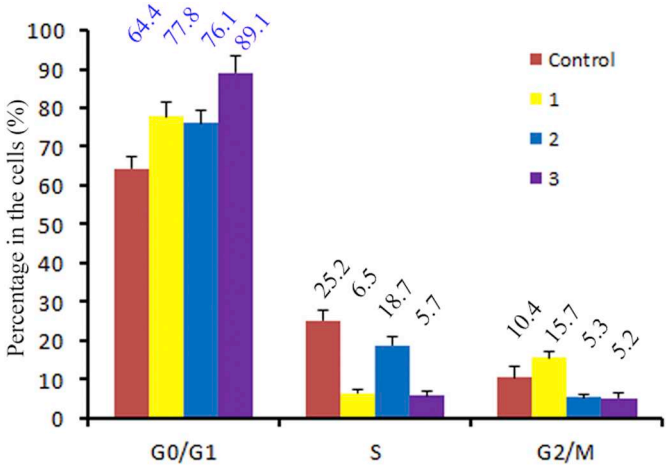


**Fig. 11.** Cell cycle distribution of A549 cells exposure to 1.2 μM of the complexes for 24 h.

apoptosis in a short time [51]. Reduction of mitochondrial membrane potential is a hallmark of early apoptosis [52,53]. To study whether the complexes target the mitochondria, MitoTracker red was used to stain mitochondria. See from Fig. 6A, the mitochondria were stained red (control, a). While the complexes emit green fluorescence after A549 cells were incubated with 1.2 μM of complexes **1** (b), **2** (c) and **3** (d) for 3 h. The merge suggests that the complexes interact with mitochondria. The Pearson's colocalization coefficient (PCC) was obtained by analyzing the red and green fluorescent intensity in 50 cells according to literature [43]. The PCC value is −0.5828, which shows a negative correlation. In the assay of mitochondrial membrane potential (MMP), JC-1 was used as fluorescence probe. See from Fig. 6B, high MMP was observed because JC-1 emits red fluorescence (control, a). However, A549 cells were incubated with 1.2 μM of complexes **1** (b), **2** (c) and **3** (d) for 24 h, low MMP was observed owing to JC-1 emitting green fluorescence. Obviously, complexes **1–3** can cause a reduction of MMP. To further observe the effect of complexes **1–3** on MMP, the values of red versus green fluorescence were measured. As shown in Fig. 6C, treatment of A549 cells with CCCP (carbonylcyanide-*m*-chlorophenylhydrazone, a positive control) and different concentration of complexes **1–3** led to a decrease of the values of red versus green fluorescence.

### 3.7. Determination of ATP content

As the most direct source of energy in cells, ATP plays a vital role in the cell growth cycle. Some functions of cells are affected by changes in intracellular ATP amounts When the cells are in apoptotic, the ATP content will decrease. In other words, a decrease in ATP levels indicates impaired or decreased mitochondrial function. As shown in Table 2, we found that the intracellular ATP level induced by the complexes reduced significantly compared with that of the control. Therefore, these data confirm that the complexes interact on the mitochondria and further promote apoptosis in A549 cells.

### 3.8. Release of cytochrome c

Cytochrome c (cyto c) give play to an important role in apoptosis, and cyto c locates between the mitochondrial outer membrane and the inner membrane. When the mitochondria have been damaged, cytochrome *c* can be released from mitochondria to the cytoplasm, which further leads to apoptosis. See from Fig. 7A and B, we discover that the

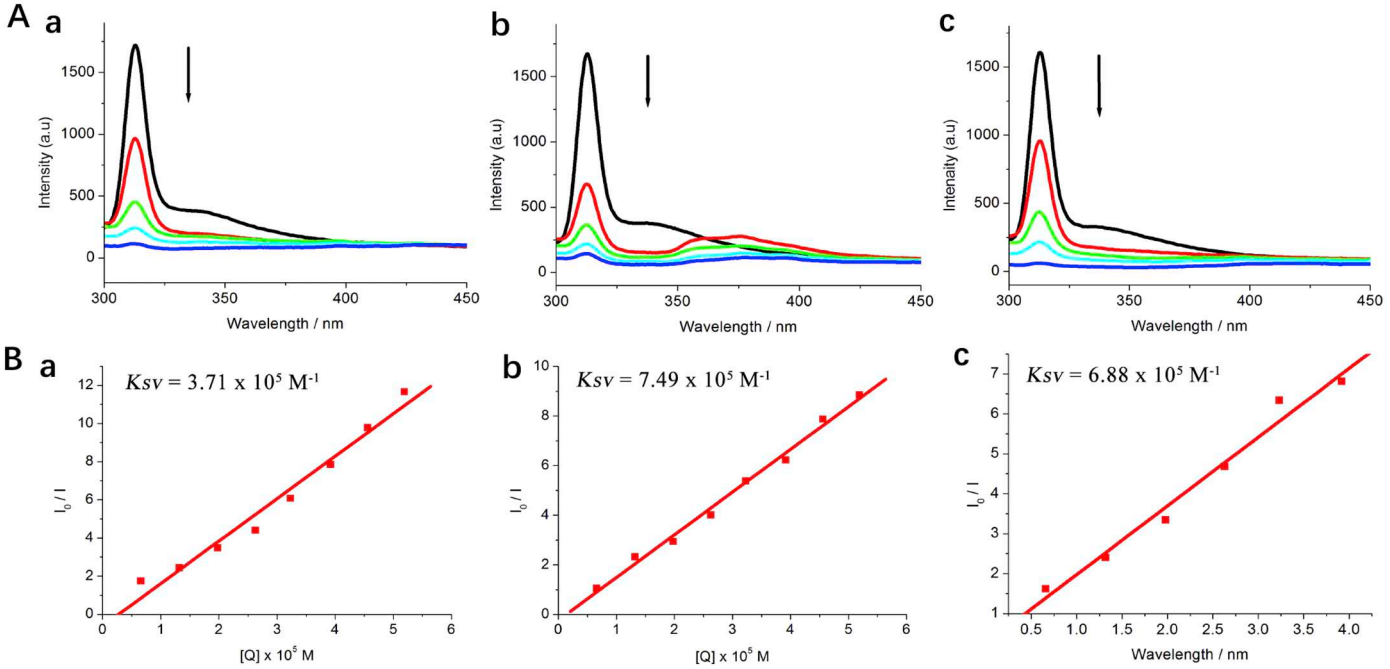


**Fig. 12.** (A) Fluorescence change of BSA with increasing amount of complexes **1** (a), **2** (b) and **3** (c). (B) The binding constants of complexes **1** (a), **2** (b) and **3** (c) interacting with BSA.

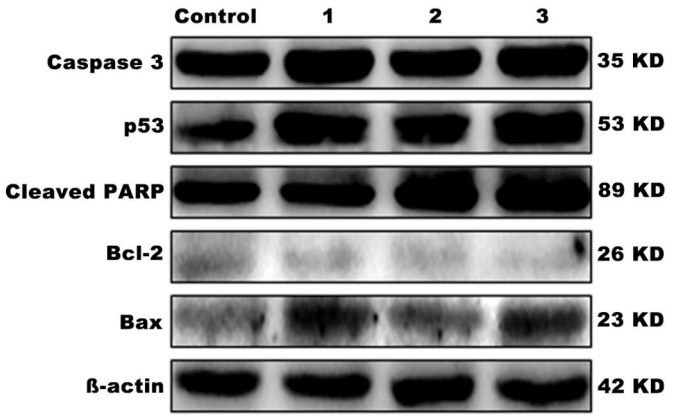


**Fig. 13.** (A) Western blot analysis of Cleaved PARP, caspase 3, p53, Bcl-2 and Bax in A549 cells treated with 1.2 μM of the complexes for 24 h. β-actin was used as internal control.

green fluorescence intensity increases 2.66 for **1**, 1.81 for **2** and 2.78 times for **3** than that in the control after A549 cells were exposed to 1.2 μM of complexes **1–3** for 24 h, which demonstrates that the complexes release cytochrome *c* in a dose-dependent manner.

### 3.9. DNA damage studies

The complexes can increase intracellular ROS levels, overproduction of reactive oxygen species can lead to DNA damage. Hence, DNA damage was carried out by comet electrophoresis. As shown in Fig. 8, in the control (a), the cells fail to show comet-like appearance and the cell nuclei show a normal roundness. After the treatment of A549 cells with $H_2O_2$ (100 μM, positive control, b) and 1.2 μM of complexes **1** (c), **2** (d) and **3** (e) for 24 h, well- formed comets were observed. The results show that the complexes can induce DNA fragmentation, providing further evidence of apoptosis.

### 3.10. Apoptosis assays using AO/EB double staining and flow cytometry

We used acridine orange (AO) and ethidium bromide (EB) to study the cell morphological changes. The viable cells show light green fluorescing nuclei with highly organized structures. in the control (Fig. 9A, a), A549 cells were exposed to 0.6 μM of complexes **1** (b), **2** (c) and **3** (d) for 24 h, apoptotic cells with apoptotic features such as nuclear shrinkage and chromatin condensation were also found. These findings reveal that the complexes can induce apoptosis in A549 cells. The apoptosis was also examined by flow cytometry. In the control (a), the percentage of the apoptotic cells is 0.86%, after 24 or 48 h of exposure of A549 cells to $IC_{50}$ value of complexes **1** (b and e), **2** (c and f) and **3** (d and g), the percentages in the early apoptotic cells are 7.86% and 8.32%, 7.28% and 12.40%, 4.22% and 7.59%, respectively (Fig. 9B). The results indicate that the complexes reveal a time-dependent manner to induce apoptosis in A549 cells.

### 3.11. Effect of the complexes on cell invasion

Invasion and metastasis of tumor cells are the main features of malignant tumors, and they are the primary factors causing the death of patients with malignant tumors [54,55]. Thus, it is necessary to evaluate the ability of the complexes to inhibit the cell invasion. See from Fig. 10A, after A549 cells (a) were treated with 0.6 μM of complexes **1** (b), **2** (c) and **3** (d) for 24 h, the number of cells passing through the basement membrane was significantly reduced compared with that in the control. To quantify the effect of the complexes on cell invasion, A549 cells were exposed to different concentration of the complexes and results are shown in Fig. 10B. Fig. 10B shows that the complexes reveal high inhibitory ability to inhibit cell invasion, the inhibitory rate for complex **3** reaches 82.1%.

### 3.12. Cell cycle distribution in A549 cells

The level of reactive oxygen species such as hydrogen peroxide in cancer cells is higher than that in normal cells, and active oxygen is very important for the progression of the cell cycle. On the other hand, DNA damage also affects the process of cell mitosis and the distribution

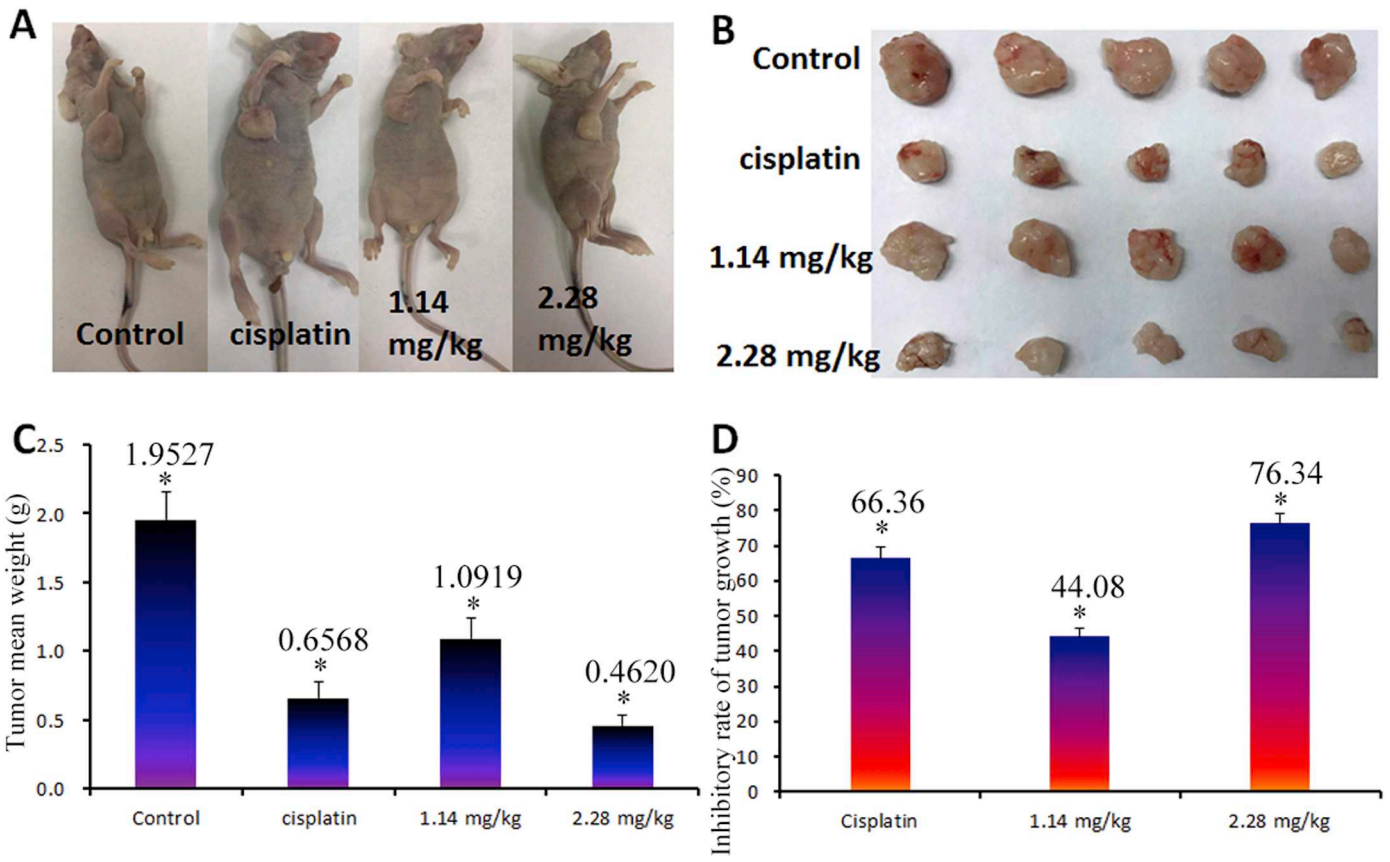


**Fig. 14.** The in vivo antitumor activity of complex **3** in A549 xenograft model. (A and B) Photographs of tumor from treatment groups and vehicle group. (C) Tumor weight (Mean ± SD) g after the tumor was treated with the complex **3** for 7 days. (D) Inhibiting percentage of tumor growth induced by cisplatin and different concentrations of complex **3**. *$P < 0.05$ represents significant differences compared with control.

of the cell cycle [56,57]. To investigate the mechanism of the complexes inhibiting cell proliferation, the cell cycle arrest was assayed by flow cytometry. As shown in Fig. 11, it is clear that there is a large change of percentage in the cells at the $G_0/G_1$ phase. The proportion of $G_0/G_1$ phase cells in the control was 64.4%, while the proportion of the cell cycle in A549 cells treated with 1.2 μM of complexes **1–3** was 77.8%, 76.1%, and 89.1%, respectively. A large increase of the percentage in the cells at the G0/G1 phase is 13.4% for **1**, 11.7% for **2** and 24.7% for **3** was observed, which was accompanied by corresponding reduction at S phase. The results indicate that the complexes inhibit the cell proliferation at $G_0/G_1$ phase.

### 3.13. BSA-binding studies

The interaction between BSA and complexes **1**, **2** and **3** was studied by a tryptophan emission-quenching experiment. Generally, the fluorescence of protein is caused by three intrinsic characteristics of the protein, namely tryptophan, tyrosine, and phenyl alanine residues. Actually, the intrinsic fluorescence of many proteins is mainly contributed by tryptophan alone [58,59]. The emission spectrum of BSA in the buffer medium (excited at 290 nm) shows a characteristic peak at 342 nm that is mainly due to the presence of tryptophan residues. See from Fig. 12A, addition of successive amounts of iridium(III) complexes **1** (a), **2** (b) and **3** (c) to BSA results in a large decrease of 93.3% for **1**, 91.4% for **2** and 96.2% for **3** in the fluorescence intensity. In order to compare quantitatively the BSA-binding affinity of the complexes to quench the emission intensity of BSA, the quenching constants were calculated by the linear Stern-Volmer equation [60].

$$I_0/I = 1 + Ksv[Q]$$

$I_0$ and I represent the fluorescence intensities in the absence and presence of quencher, respectively. *Ksv* is a linear Stern-Volmer quenching constant, [Q] is the concentration of the complexes. The static mechanism usually results from ground-state complex formation between the quencher and fluorophore, it causes perturbation of the absorption spectrum of the fluorophore. Therefore, we use corrected $I_0/I$ values to calculate *Ksv* [61–63]. From the quenching plot of $I_0/I$ versus [Q] (Fig. 12B), *Ksv* of complexes **1** (a), **2** (b) and **3** (c) are obtained from the slope. The calculated values of *Ksv* for the interaction of **1**, **2** and **3** with BSA are 3.71 ( ± 0.15) × $10^5$ $M^{-1}$, 7.49 ( ± 0.31) × $10^5$ $M^{-1}$and 6.88 ( ± 0.40) × $10^5$ $M^{-1}$, which indicates high BSA binding affinity of the complexes with protein and follows the order of **2** > **3** > **1**.

### 3.14. The expression of caspase 3, p53, cleaved PARP, Bcl-2 and Bax

Through the above experiments, we learned that the three complexes can cause changes in the physiological environment within the cell and lead to apoptosis. Moreover, the complexes show high protein affinity, therefore, we used immunoblot to investigate the expression of apoptotic-related proteins. Bcl-2 family proteins, including anti-apoptotic and pro-apoptotic proteins, play an important role in the regulation of cell apoptosis. As shown in Fig. 13, treatment of 24 h of A549 cells with the complexes led to a decrease in the expression of Bcl-2 and an increase in the expression of Bax protein compared with that in the control. In addition, the expression level of the apoptotic executive protein caspase 3 and cleaved-PARP increased, and the expression of p53 protein was up-regulated, which indicated that the complexes can inhibit DNA replication and restrict mitosis.

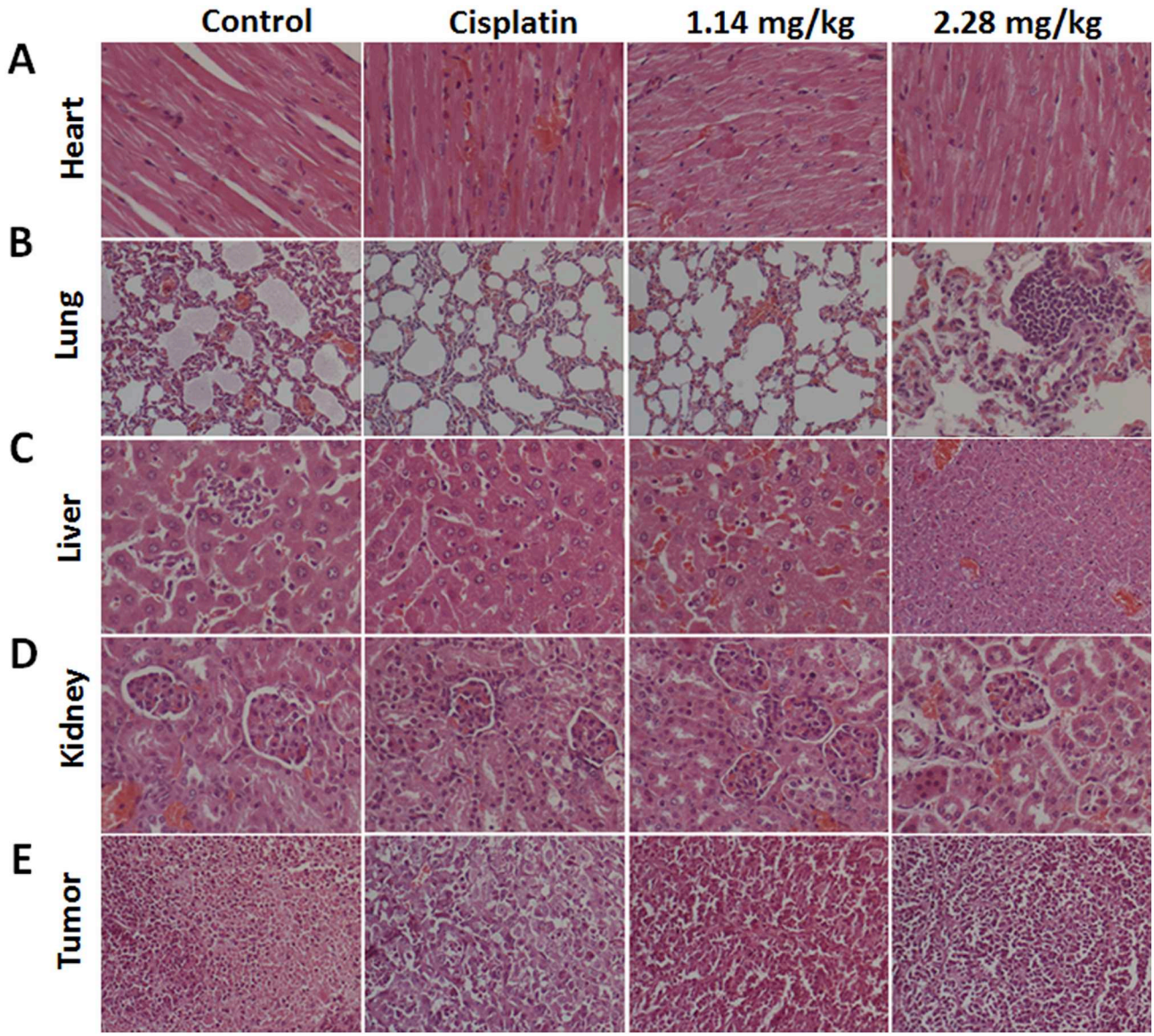


**Fig. 15.** Effect of cisplatin and the complex **3** on the tissue: (A) Mild edema and congestion in the interstitial tissue of myocardial cells in the groups of control, cisplatin, 1.14 mg/kg and 2.28 mg/kg complex **3**; (B) Slight congestion in the interstitial tissues of alveoli showed in all groups; (C) Liver cells showed mild edema and cytoplasmic loose in all groups; (D) Mild edema in renal tubule and glomerular cells in all groups; (E) More poorly differentiated adenocarcinoma, hemorrhage and necrosis showed in groups of cisplatin and complex **3** (1.14 mg/kg and 2.28 mg/kg) compared to the control group.

### *3.15. Evaluation of antitumor activity in vivo and effect of the complexes on tissues*

Complex **3** shows high anticancer activity in vitro against A549 cells. This prompts us to investigate the antitumor activity in vivo. Xenograft tumors were obtained by eight consecutive days of subcutaneous implantation of A549 cells into nude mice. Cisplatin (2 mg/kg) was used as a positive control. Treatment of the mice with 1.14 mg/kg or 2.28 mg/kg of complex **3** every day, the body weights and relative volume of the mice were obtained. See from Fig. 14A-D, the average weight of tumor treated with 2.28 mg/kg of complex **3** is smaller than those of control and cisplatin. The inhibitory rate of cisplatin toward xenograft tumors is 66.36%, whereas the inhibitory rate caused by 2.28 mg/kg of **3** reaches 76.34%. In addition, the morphology of heart, liver, kidney, lung and tumor tissue was observed by H&E (Hematoxylin-Eosin) staining. Cisplatin and complex **3** induced mild cardiac myocyte edema and interstitial hyperemia, similar to the control group (Fig. 15A). Slight congestion in the interstitial tissues of alveoli were also found in all groups (Fig. 15B). In all groups, slight hepatocyte edema, small focal necrosis (Fig. 15C) and mild renal tubular epithelial edema (Fig. 15D) was observed. However, cisplatin, 1.14 mg/kg and 2.28 mg/kg of complex **3** induced more focal necrosis of adenocarcinoma in tumor tissue compared to the control group (Fig. 15E). Hence, we think that complex **3** targets the tumor tissue, and this complex may be potent anticancer drug candidate.

## 4. Conclusions

In this paper, three new iridium(III) complexes were synthesized and characterized. Their anticancer activities in vitro were studied. Complexes **1**, **2** and **3** show high anticancer activity against A549 cells than cisplatin under the same conditions, and the complexes can effectively inhibit the cell invasion and cell proliferation. The complexes target the lysosomes and cause the increase of lysosomal permeabilization. Complexes **1**–**3** can increase the intracellular ROS levels, enhance the concentrations of intracellular $Ca^{2+}$, and induce a decrease of the mitochondrial membrane potential and ATP amounts, further induce a release of cytochrome *c*, activate caspase 3. Additionally, the

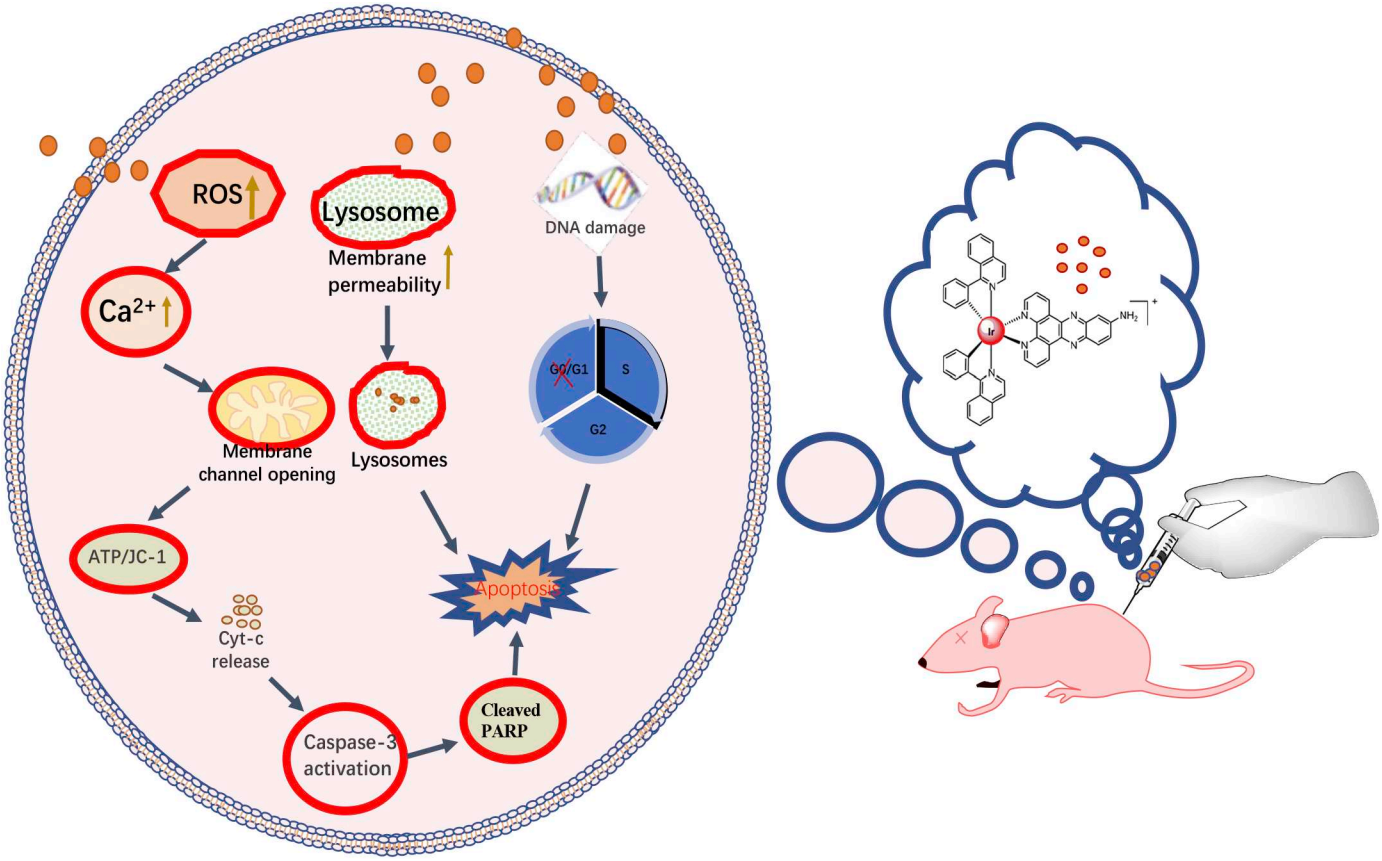


**Fig. 16.** The mechanism of the complexes inducing apoptosis in A549 cells.

complexes can damage DNA, inhibit the cell growth at G0/G1 phase. Antitumor activity in vivo demonstrates that complex **3** (2.28 mg/kg) can effectively inhibit the tumor growth, and its efficiency is higher than cisplatin. The complexes have no effect on the heart, liver, kidney and lung tissues, but the complexes can target the tumor tissue. In summary, we consider that the complexes induce apoptosis in A549 cells through the following three pathways (Fig. 16): (I) The complexes target the lysosomes and increase lysosomal permeabilization; (II) After the complexes interact on the cells, which causes an dramatic increase of the intracellular ROS content, enhances intracellular $Ca^{2+}$ concentration, then complexes keep the mitochondrial permeability transmembrane channel open, which in turn reduces the mitochondrial membrane potential, promotes the release of cytochrome *c* to the cytosol, activates caspase 3, finally, cause apoptosis; (III) The complexes cause DNA damage, and inhibit the cell growth at G0/G1 phase. Consequently, we think the complexes may be potent anticancer drugs for A549 cells. This work is helpful for designing and synthesizing new iridium(III) complexes as potent anticancer drugs.

## Declaration of competing interest

Authors declare that no competing interest exists.

## Acknowledgements

This work was supported by the National Natural Science Foundation of China (Nos 21877018, 81770527), Natural Science Foundation of Guangdong Province (Nos 2016A030313724, 2016A030313728).

## References

[1] N. Kerru, P. Singh, N. Koorbanally, R. Raj, V. Kumar, Eur. J. Med. Chem. 142 (2017) 179–212.
[2] M. Nagaraju, E.G. Deepthi, C. Ashwini, M.V.P.S. Vishnuvardhan, V.L. Nayak, R. Chandra, S. Ramakrishna, B.B. Gawali, Bioorg. Med. Chem. Lett. 22 (2012) 4314–4317.
[3] T.A. Skolarus, A. Wolf, N.L. Erb, D.D. Brooks, B.M. Rivers, W. Underwood, A.L. Salner, M.J. Zelefsky, J.B. Aragon-Ching, S.F. Slovin, D.A. Wittmann, M.A. Hoyt, V.J. Sinibaldi, G. Chodak, M.L. Pratt-Chapman, R.L. Cowens-Alvarado, American Cancer Society prostate cancer survivorship care guidelines, CA Cancer J. Clin. 64 (2014) 225–249.
[4] S. Dasari, P.B. Tchounwou, Eur. J. Pharm. 740 (2014) 364–378.
[5] M.A. Jakupec, M. Galanski, V.B. Arion, G.C. Hartinger, B.K. Keppler, Dalton Trans. (2) (2008) 183–194.
[6] X.Y. Zhang, M. Zhang, Q. Cong, M.X. Zhang, M.Y. Zhang, Y.Y. Lu, C.J. Xu, Int. J. Biochem. Cell Biol. 95 (2018) 9–16.
[7] M. Markman, Expert Opin. Drug Saf. 2 (2003) 597–607.
[8] A.K. Singh, D.S. Pandey, Q. Xu, P. Braunstein, Coord. Chem. Rev. 270 (2014) 31–56.
[9] Y. Han, W. Yin, J.J. Li, H. Zhao, Z.S. Zha, W.D. Ke, Y.H. Wan, C.X. He, Z.S. Ge, J. Control. Release 273 (2018) 30–39.
[10] N.H. Ferreira, R.A. Furtado, A.B. Ribeiro, P.F. Oliveira, S.D. Ozelin, L.D.R. Souza, F.R. Neto, B.A. Miura, G.M. Magalhães, E.J. Nassar, D.C. Tavares, J. Inorg. Biochem. 182 (2018) 9–17.
[11] W.L. Zhang, L.L. Zhao, J. Liu, J. Du, Z.C. Wang, C.G. Ruan, K.S. Dai, Thromb. Res. 130 (2012) 81–91.
[12] S.W. Wang, Y. Xu, Y.Y. Weng, X.Y. Fan, Y.F. Bai, Y.F. Zheng, L.J. Lou, F. Zhang, Food Chem. Toxicol. 114 (2018) 227–236.
[13] H.Y. Yin, Q.Q. Yang, Z.X. Cao, H.R. Li, Z.Y. Yu, G.D. Zhang, G.Y. Sun, R.J. Man, H.B. Wang, J.F. Li, Toxicol. Appl. Pharm. 343 (2018) 16–28.
[14] V.L. Bodiga, M.R. Kudle, S. Bodiga, Biochem. Pharmacol. 98 (2015) 78–91.
[15] G. Akca, H. Eren, L. Tumkaya, T. Mercantepeb, M.O. Horsanalic, E. Devecid, E. Dila, A. Yilmaze, Biomed. Pharmacother. 100 (2018) 575–582.
[16] S. Choudhary, S. Sood, H.R. Wang, Biochem. Biophys. Res. Commun. 436 (2013) 325–330.
[17] B. Rosenberg, V. Camp, E.B. Grimley, J. Biol. Chem. 242 (1967) 1347–1352.
[18] Z.Q. Huang, G.T. Yang, T. Shen, X.N. Wang, H.Z. Li, D.M. Ren, Biomed. Pharmacother. 89 (2017) 623–631.
[19] L. He, S.Y. Liao, C.P. Tan, Y.Y. Lu, C.X. Xu, L.N. Ji, Z.W. Mao, Chem. Commun. 50 (2014) 5611–5614.

[20] S.K. Tripathy, U. De, N. Dehury, P. Laha, M.K. Panda, H.S. Kim, S. Patra, Dalton Trans. 45 (2016) 15122–15136.
[21] Z.D. Mou, N. Deng, F. Zhang, J.Y. Zhang, J. Cen, X. Zhang, Eur. J. Med. Chem. 138 (2017) 72–82.
[22] C. Zhang, S.H. Lai, C.C. Zeng, B. Tang, D. Wan, D.G. Xing, Y.J. Liu, J. Biol. Inorg. Chem. 21 (2016) 1047–1060.
[23] G. Ludwig, S. Mijatović, I. RanCelović, M. Bulatović, D. Miljković, D. MaksimovićIvanić, M. Korb, H. Lang, D. Steinborn, G.N. KaluCerović, Eur. J. Med. Chem. 69 (2013) 216–222.
[24] R.P. Paitandi, R.K. Gupta, R.S. Singh, G. Sharma, B. Koch, D.S. Pandey, I Eur. J. Med. Chem. 84 (2014) 17–29.
[25] M.J. Berridge, M.D. Bootman, H.L. Roderick, Nat. Rev. Mol. Cell Biol. 4 (2003) 517–529.
[26] M.H. Chen, F.X. Wang, J.J. Cao, C.P. Tan, L.N. Ji, Z.W. Mao, ACS Appl. Mater. Inter. 9 (2017) 13304–13314.
[27] C.L. Wang, J.F. Liu, Z.Z. Tian, L.J. Tian, W.Q. Zhao, Z. Liu, Dalton Trans. 46 (2017) 6870–6883.
[28] W.L. Ma, L.H. Guo, Z.Z. Tian, S.M. Zhang, X.D. He, J.J. Li, Y.L. Yang, Z. Liu, Dalton Trans. 48 (2019) 4788–4893.
[29] Z.Z. Tian, J.J. Li, S.M. Zhao, Z.S. Xu, Y.L. Yang, D.L. Kong, H.R. Zhang, X.X. Ge, J.M. Zhang, Z. Liu, Inorg. Chem. 57 (2018) 10498–10502.
[30] J. Yang, J.X. Zhao, Q. Cao, L. Hao, D.X. Zhou, Z.J. Gan, L.N. Ji, Z.W. Mao, ACS Appl. Mater. Inter. 9 (2017) 13900–13912.
[31] G.J. Lin, Z.Z. Li, J.H. Yao, H.L. Huang, Y.Y. Xie, Y.J. Liu, Aust. J. Chem. 66 (2013) 555–567.
[32] Y.Y. Xie, Z.Z. Li, G.J. Lin, H.L. Huang, X.Z. Wang, Z.H. Liang, G.B. Jiang, Y.J. Liu, Inorg. Chim. Acta 405 (2013) 228–234.
[33] G.J. Lin, G.B. Jiang, Y.Y. Xie, H.L. Huang, Z.H. Liang, Y.J. Liu, J. Biol. Inorg. Chem. 18 (2013) 873–882.
[34] W.Y. Zhang, Y.J. Wang, F. Du, Y.Y. Gu, L. Bai, L.L. Yang, Y.J. Liu, Eur. J. Med. Chem. 178 (2019) 401–416.
[35] S. Sprouse, K.A. King, P.J. Spellane, R.J. Watts, Am. Chem. Soc. 106 (1984) 6647–6653.
[36] T. Mosmann, J. Immunol. Methods 65 (1983) 55–63.
[37] R.H. Cao, Q. Chen, X.R. Hou, H.S. Chen, H.J. Guan, Y. Ma, W.L. Peng, A.L. Xu, Bioorg. Med. Chem. 12 (2004) 4613–4623.
[38] B. Tang, D. Wan, Y.J. Wang, Q.Y. Yi, B.H. Guo, Y.J. Liu, Eur. J. Med. Chem. 145 (2018) 302–314.
[39] Q.Y. Yi, D. Wan, B. Tang, Y.J. Wang, W.Y. Zhang, F. Du, M. He, Y.J. Liu, Eur. J. Med. Chem. 145 (2018) 338–349.
[40] S. Fakih, M. Podinovskaia, X. Kong, H.L. Collins, U.E. Schaible, R.C. Hider, J. Med. Chem. 51 (2008) 4539–4552.
[41] J.P. Falgueyret, S. Desmarais, R. Oballa, W.C. Black, W. Cromlish, K. Khougaz, S. Lamontagne, F. Masse, D. Riendeau, S. Toulmond, M.D. Percival, J. Med. Chem. 48 (2005) 7535–7543.
[42] R. Gigli, G.J.S. Pereira, F. Antunes, A. Bechara, D.M. Garcia, D.G. Spindola, M.G. Jasiulionis, A.C.F. Caires, S.S. Smaili, C. Bincoletto, Eur. J. Med. Chem. 107 (2016) 245–254.
[43] J. Adler, I. Parmryd, Cytom. Part A 77A (2010) 733–742.
[44] M.J. Berridge, M.D. Bootman, P. Lipp, Nature 395 (1998) 645–648.
[45] W. Capoen, J. Sun, D. Wysham, M.S. Otegui, M. Venkateshwaran, S. Hirsch, H. Miwa, J.A. Downie, R.J. Morris, J.M. Ane, G.E.D. Oldroyd, Proc. Natl. Acad. Sci. U. S. A. 108 (2011) 14348–14353.
[46] V. Konieczny, M.V. Keebler, C.W. Taylor, Semin. Cell Dev. Biol. 23 (2012) 172–180.
[47] Q.L. Liu, H.Z. Du, X.Z. Ren, W. Bian, L. Fan, S.M. Shuang, C. Dong, Q. Hu, M.M.F. Choi, Anal. Chem. 86 (2014) 8025–8030.
[48] C. Camello-Almaraz, P.J. Gomez-Pinilla, M.J. Pozo, P.J. Camello, Am. J. Physiol-Cell Ph. 291 (2006) C1082–C1088.
[49] C. Cerella, M. Diederich, L. Ghibelli, Int. J. Cell Biol. 2010 (2010) 546163.
[50] A. Heller, G. Brockhoff, A. Goepferich, Eur. J. Pharm. Biopharm. 82 (2012) 1–18.
[51] K. Sinha, J. Das, P.B. Pal, P.C. Sil, Arch. Toxicol. 87 (2013) 1157–1180.
[52] J.S. Armstrong, Br. J. Pharmacol. 151 (2007) 1154–1165.
[53] R. Clayton, J.B. Clark, Neurochem 92 (2005) 840–849.
[54] P. Morais, M. Reichard, Sci. Total Environ. 613–614 (2018) 1438–1448.
[55] P. Courtois, C. Figuieres, C. Mulier, J. Weill, Ecol. Econ. 146 (2018) 607–620.
[56] F. Sultana, S.R. Bonam, V.G. Reddy, V.L. Nayak, R. Akunuri, S.R. Routhua, A. Alarifie, M. Sampath, K. Halmuthur, A. Kamal, Bioorg. Chem. 76 (2018) 1–12.
[57] N.P. Kumar, P. Sharma, S.S. Kumari, U. Brahm, S. Nekkanti, N. Shankaraiah, A. Kamal, Eur. J. Med. Chem. 140 (2017) 128–140.
[58] T. Peters, Serum albumin, Adv. Protein Chem. 37 (1985) 161–245.
[59] K. Karami, M. Hosseini-Kharat, H. Sadeghi-Aliabadi, J. Lipkowski, M. Mirian, Eur. J. Med. Chem. 73 (2014) 8–17.
[60] Y.J. Hu, Y. Liu, J.B. Wang, X.H. Xiao, S.S. Qu, J. Pharm. Biomed. Anal. 36 (2004) 915–919.